Article

Immunity

Cholesterol Homeostatic Regulator SCAP-SREBP2 Integrates NLRP3 Inflammasome Activation and Cholesterol Biosynthetic Signaling in Macrophages

Graphical Abstract

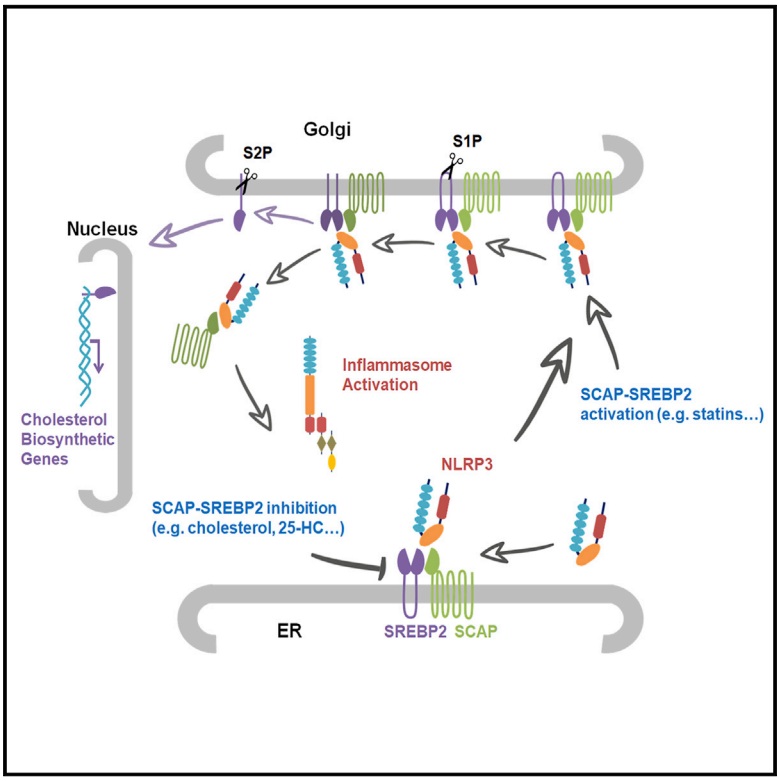

Authors

Chuansheng Guo, Zhexu Chi, Danlu Jiang, ..., Yingliang Wu, Bao-Liang Song, Di Wang

Correspondence

diwang@zju.edu.cn

In Brief

The metabolic-inflammatory crosstalk plays a key role in host defense against pathogens and inflammation. Guo and colleagues demonstrate that SCAP-SREBP2 complex integrates NLRP3 inflammasome activation and cholesterol biosynthetic signaling during inflammation.

Highlights

- NLRP3 inflammasome activation couples SREBP2 maturation
- SCAP-SREBP2 translocation and S1P are required for optimal NLRP3 inflammasome activity
- SCAP escorts both NLRP3 and SREBP2 by forming a ternary complex
- SCAP-SREBP2 inhibition protects mice from systemic inflammation

Guo et al., 2018, Immunity *49*, 1–15
November 20, 2018
https://doi.org/10.1016/j.immuni.2018.08.021

CellPress

Please cite this article in press as: Guo et al., Cholesterol Homeostatic Regulator SCAP-SREBP2 Integrates NLRP3 Inflammasome Activation and Cholesterol Biosynthetic Signaling in Macrophages, Immunity (2018), https://doi.org/10.1016/j.immuni.2018.08.021

Immunity
Article

Cholesterol Homeostatic Regulator SCAP-SREBP2 Integrates NLRP3 Inflammasome Activation and Cholesterol Biosynthetic Signaling in Macrophages

Chuansheng Guo,[1,2,6] Zhexu Chi,[1,2,6] Danlu Jiang,[1,2,6] Ting Xu,[1,2] Weiwei Yu,[4] Zhen Wang,[1,2] Sheng Chen,[1,2] Li Zhang,[1,2] Qianyun Liu,[4] Xingchen Guo,[4] Xue Zhang,[2,3] Wenxin Li,[4] Linrong Lu,[1,2] Yingliang Wu,[4] Bao-Liang Song,[5] and Di Wang[1,2,7,*]
[1]Institute of Immunology, Zhejiang University School of Medicine, Hangzhou 310058, P.R. China
[2]Program in Molecular and Cellular Biology, Zhejiang University School of Medicine, Hangzhou 310058, P.R. China
[3]Department of Pathology and Pathophysiology, Zhejiang University School of Medicine, Hangzhou 310058, P.R. China
[4]State Key Laboratory of Virology, College of Life Sciences, Wuhan University, Wuhan 430072, P.R. China
[5]Hubei Key Laboratory of Cell Homeostasis, College of Life Sciences, Wuhan University, Wuhan 430072, P.R. China
[6]These authors contributed equally
[7]Lead Contact
*Correspondence: diwang@zju.edu.cn
https://doi.org/10.1016/j.immuni.2018.08.021

SUMMARY

Cholesterol metabolism has been linked to immune functions, but the mechanisms by which cholesterol biosynthetic signaling orchestrates inflammasome activation remain unclear. Here, we have shown that NLRP3 inflammasome activation is integrated with the maturation of cholesterol master transcription factor SREBP2. Importantly, SCAP-SREBP2 complex endoplasmic reticulum-to-Golgi translocation was required for optimal activation of the NLRP3 inflammasome both *in vitro* and *in vivo*. Enforced cholesterol biosynthetic signaling by sterol depletion or statins promoted NLPR3 inflammasome activation. However, this regulation did not predominantly depend on changes in cholesterol homeostasis controlled by the transcriptional activity of SREBP2, but relied on the escort activity of SCAP. Mechanistically, NLRP3 associated with SCAP-SREBP2 to form a ternary complex which translocated to the Golgi apparatus adjacent to a mitochondrial cluster for optimal inflammasome assembly. Our study reveals that, in addition to controlling cholesterol biosynthesis, SCAP-SREBP2 also serves as a signaling hub integrating cholesterol metabolism with inflammation in macrophages.

INTRODUCTION

The immune and metabolic systems are highly integrated with one another, and this is critical for immune cells to fulfill their functions. A hallmark of pro-inflammatory macrophages is the increased anabolic demand in response to pathogen- or damage-associated molecular patterns (PAMPs or DAMPs) (O'Neill et al., 2016; Pearce and Pearce, 2013). The NLRP3 inflammasome is a molecular platform that modulates innate immune functions via the maturation of caspase-1 and via the cleavage of cytokine substrates such as pro-interleukin (IL)-1β and pro-IL-18 (Rathinam and Fitzgerald, 2016). Recent studies have implicated several cellular metabolites and metabolic enzymes, traditionally linked to metabolism but not immunity, in modulation of NLRP3 inflammasome activation (Próchnicki and Latz, 2017).

Cholesterol is an essential lipid involved in diverse biological processes (Tall and Yvan-Charvet, 2015). Excess cholesterol can form cholesterol crystals, which directly activate the NLRP3 inflammasome and underlie the pathogenesis of atherosclerosis (Duewell et al., 2010). Cholesterol accumulation in dendritic cells accelerates the development of autoimmunity via the NLRP3 inflammasome, possibly at the transcriptional level (Ito et al., 2016; Westerterp et al., 2017). However, the molecular mechanisms that directly link cholesterol metabolic signaling and NLRP3 inflammasome activation remain poorly defined.

The sterol regulatory element-binding proteins (SREBPs) are master regulators of lipid homeostasis (Goldstein et al., 2006). Mammals have two SREBP-encoding genes that express three SREBPs: SREBP1a, SREBP1c, and SREBP2. SREBP2 principally regulates genes involved in cholesterol metabolism, whereas genes involved in fatty-acid metabolism are preferentially regulated by SREBP1. They are synthesized as inactive precursors localized to the endoplasmic reticulum (ER) bound to SREBP cleavage-activating protein (SCAP). SCAP escorts SREBPs via coat protein complex II (COPII) vesicles to the Golgi apparatus where two steps of proteolytic cleavage mediated by Site-1 protease (S1P) and Site-2 protease (S2P) releases the N terminus of SREBP protein and allows its entry into the nucleus (Goldstein et al., 2006).

In the current study, we found that SCAP-SREBP2 promoted NLRP3 inflammasome activation, which was mainly dependent on its ER-to-Golgi translocation, rather than by affecting cholesterol homeostasis. By inhibiting this translocation, synthetic SCAP-SREBP2 inhibitors and endogenous sterols including cholesterol and 25-HC suppressed NLRP3 inflammasome activation both *in vitro* and *in vivo*. In contrast, cholesterol depletion or statins promoted NLRP3 inflammasome activation by enforcing this process. Collectively, we unveil an important role of SCAP-SREBP2 that is directly used by NLRP3 for inflammasome

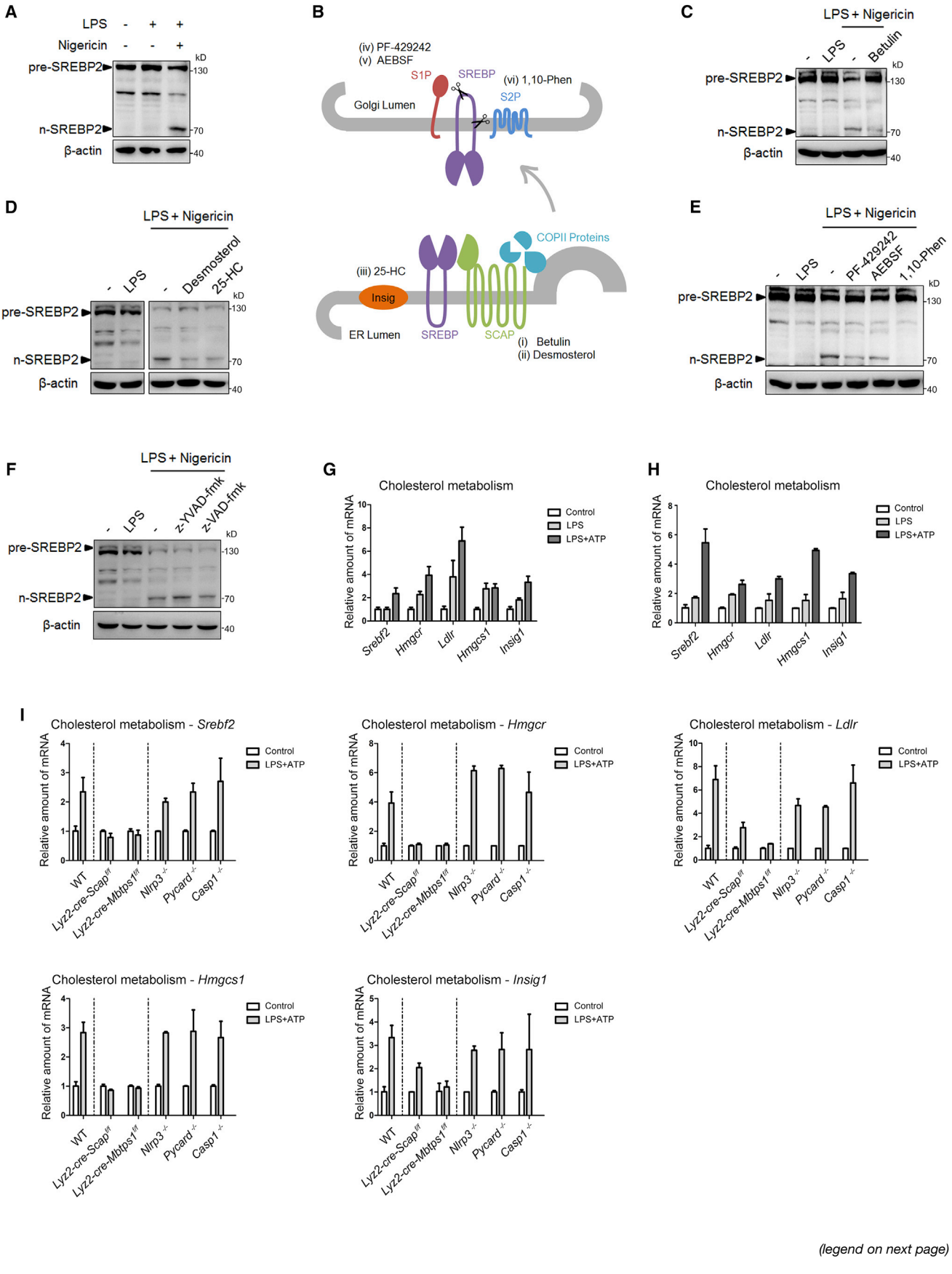

(legend on next page)

activation, thus suggesting an intimate metabolic-inflammatory crosstalk in pro-inflammatory macrophages.

RESULTS

NLRP3 Inflammasome Activation Couples SCAP ER-to-Golgi Translocation and SREBP2 Maturation

Upon nigericin stimulation in lipopolysaccharide (LPS)-primed THP1 macrophages, we found that the SREBP2 inactive precursor (pre-SREBP2) was clearly proteolytically processed to the N-terminal mature form (n-SREBP2) (Figure 1A). To determine whether this nigericin-induced SREBP2 processing occurred via the well-established SCAP-, S1P-, and S2P-dependent pathway, we used several synthetic inhibitors and endogenous sterols targeting this pathway (Figure 1B). Betulin, a small molecule that specifically inhibits SCAP-SREBP2 activation by interacting with SCAP (Tang et al., 2011), suppressed this nigericin-induced cleavage of SREBP2 (Figure 1C). Desmosterol binds to SCAP and prevents it from interacting with COPII proteins, which results in the retention of SCAP-SREBP2 in the ER. In contrast, the oxysterol 25-HC binds to the ER-retention proteins Insig1 and/or Insig2, thereby causing SCAP-SREBP2 to also be retained in the ER (Spann and Glass, 2013). We found that either desmosterol or 25-HC suppressed this nigericin-induced SREBP2 maturation (Figure 1D). Furthermore, S1P inhibition by PF-429242 or AEBSF and S2P inhibition by 1,10-phenanthroline (Feng et al., 2007; Okada et al., 2003; Shao and Espenshade, 2014) were capable of suppressing this nigericin-induced SREBP2 maturation (Figure 1E). Altogether, these findings suggested that this SREBP2 maturation occurring during NLRP3 inflammasome activation also relied on SCAP and the sequential processing by S1P and S2P. In contrast, treatment with the caspase-1 inhibitor z-YVAD-fmk or the pan-caspase inhibitor z-VAD-fmk had limited effects on this SREBP2 maturation (Figure 1F). To further strengthen these results in primary macrophages, we measured the mRNA expression of SREBP2 target genes as indicative of SREBP2 maturation, including *Srebf2* which is a direct target of itself (Sato et al., 1996). Our data showed that the five measured genes involved in cholesterol metabolism, *Srebf2*, *Hmgcr*, *Ldlr*, *Hmgcs1*, and *Insig1*, were modestly increased in LPS-primed bone marrow-derived macrophages (BMDMs) and then further enhanced upon ATP or nigericin stimulation (Figures 1G and S1A). Similar results were obtained in LPS-primed mouse peritoneal macrophages upon ATP stimulation (Figure 1H). In contrast, the caspase-1 inhibitor VX765 had no effect on the upregulation of these SREBP2 target genes (Figure S1A). Consistently, SCAP or S1P deficiency in BMDMs blocked this upregulation of SREBP2 target genes, whereas NLRP3, ASC, or Caspase-1 deficiency showed less effect on that, further suggesting that SREBP2 maturation may not depend on NLRP3 inflammasome activation in macrophages (Figure 1I). In contrast, the six measured genes involved in fatty-acid metabolism, *Srebf1*, *Acly*, *Acaca*, *Fasn*, *Acss2*, and *Gpam*, were less affected during NLRP3 inflammasome activation in BMDMs (Figure S1B). In addition, *Scap* and cholesterol efflux genes including *Abca1* and *Abcg5* were largely unchanged (Figure S1C).

Taken together, our data demonstrate that activation of the NLRP3 inflammasome is coupled with SCAP ER-to-Golgi translocation and SREBP2 maturation.

Inhibition of SCAP-SREBP2 ER-to-Golgi Translocation Impairs NLRP3 Inflammasome Activation

We next examined the role of SCAP-SREBP2 in NLRP3 inflammasome activation by acute inhibition of its ER-to-Golgi translocation (Figure 2A). Betulin, which inhibits SCAP-SREBP2 ER-to-Golgi translocation by interacting with SCAP, markedly suppressed ATP-induced caspase-1 maturation and IL-1β or IL-18 secretion in a dose-dependent manner (Figures 2B and 2C). Apart from ATP, betulin also inhibited the caspase-1 maturation and IL-1β secretion triggered by the NLRP3 agonists nigericin, monosodium urate crystals (MSU), and alum (Figures 2D and 2E). In addition, ASC (apoptosis-associated speck-like protein containing a CARD) nucleation-induced oligomerization and ASC-speck formation were also inhibited by betulin (Figures 2F and 2G). In contrast, betulin had no effect on activation of the AIM2 and NLRC4 inflammasomes, which are triggered by poly(dA:dT) transfection and *Salmonella typhimurium* infection, respectively (Figures 2H and 2I). Another selective synthetic inhibitor of SCAP-SREBP2 ER-to-Golgi translocation via binding to SCAP, fatostatin (Kamisuki et al., 2009), similarly inhibited activation of the NLRP3 inflammasome (Figures 2J and 2K). We reasoned that the suppressed NLRP3 inflammasome activity might be explained by a perturbation in cellular cholesterol homeostasis. However, the cellular cholesterol amounts and viability remained unchanged after treatment of these inhibitors (Figures S2A and S2B). We also examined these inhibitory effects of betulin and fatostatin on NLRP3 inflammasome activation in human monocyte-derived macrophages and found similar results (Figures S2C and S2D).

We next investigated this regulation of the NLRP3 inflammasome using two endogenous sterols that directly inhibit SCAP-SREBP2 ER-to-Golgi translocation: 25-HC and cholesterol itself. We found that 25-HC dose dependently repressed ATP- or

Figure 1. NLRP3 Inflammasome Activation Couples SCAP ER-to-Golgi Translocation and SREBP2 Maturation

(A) Immunoblotting of SREBP2 expression in LPS-primed THP1 macrophages stimulated with nigericin for 30 min.

(B) Schematic of the synthetic inhibitors and endogenous sterols targeting different stages of SCAP-SREBP2 activation.

(C–E) Immunoblotting of SREBP2 expression in LPS-primed THP1 macrophages treated with 5 μM betulin (C), 20 μM desmosterol or 50 μM 25-HC (D), and 200 μM PF-429242, 50 μM AEBSF, or 0.5 mM 1,10-phenanthroline (E) for 30 min (C), 3 hr (D), or 1 hr (E) and then stimulated with nigericin for 30 min.

(F) Immunoblotting of supernatants (SN) and cell extracts (Lysate) from LPS-primed THP1 macrophages treated with 20 μM z-YVAD-fmk or 20 μM z-VAD-fmk for 30 min, and then stimulated with nigericin for 30 min.

(G and H) qPCR for expression of the indicated genes in LPS-primed BMDMs (G) and peritoneal macrophages (D) stimulated with ATP for 45 min.

(I) qPCR for expression of the indicated genes in LPS-primed BMDMs from wild-type, *Lyz2-cre-Scap*$^{f/f}$, *Lyz2-cre-Mbtps1*$^{f/f}$, *Nlrp3*$^{-/-}$, *Asc*$^{-/-}$, and *Casp1*$^{-/-}$ mice stimulated with ATP for 45 min.

Data are representative of three independent experiments. See also Figure S1.

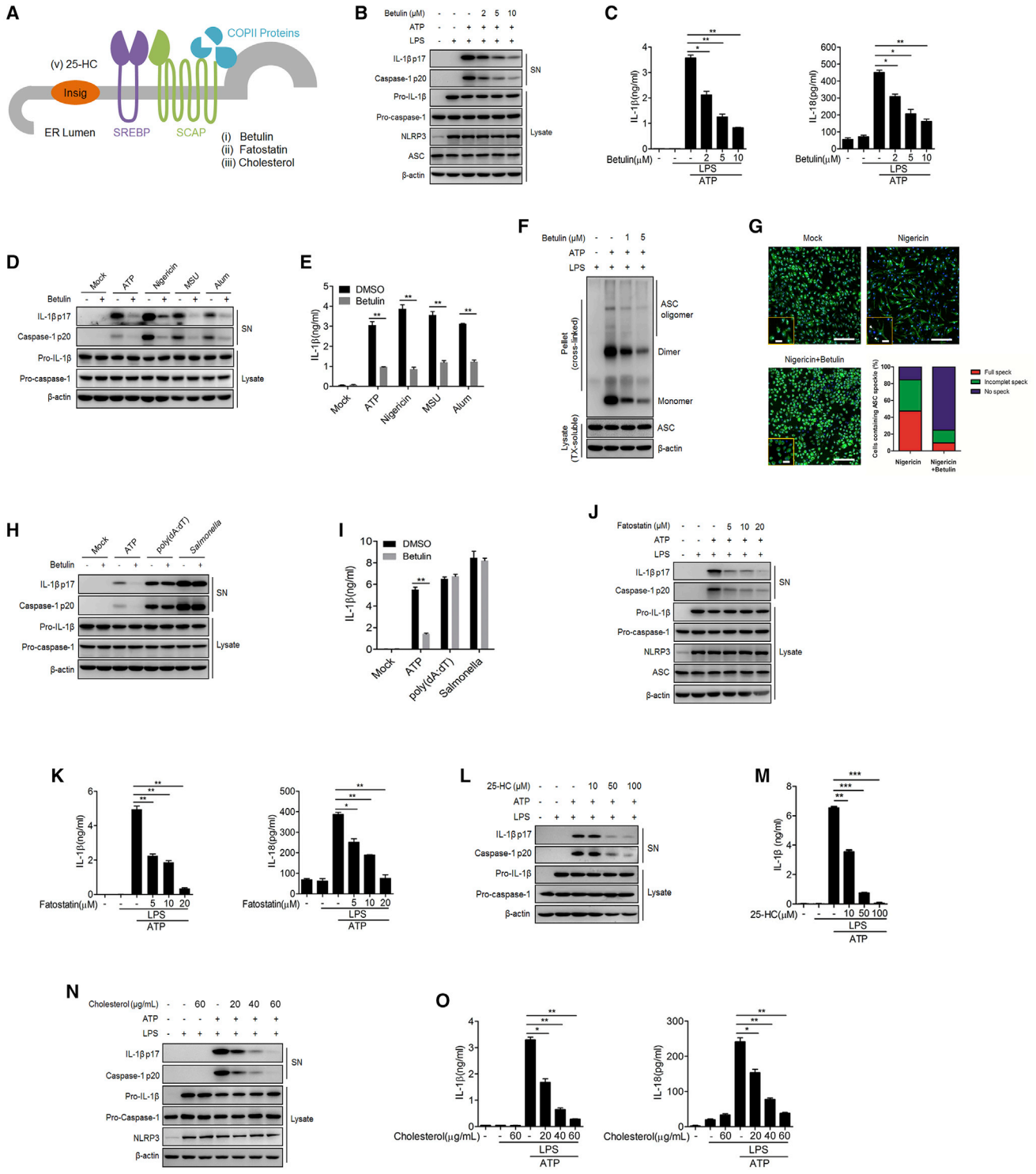

Figure 2. Inhibition of SCAP-SREBP2 ER-to-Golgi Translocation Impairs NLRP3 Inflammasome Activation

(A) Schematic of the synthetic inhibitors and endogenous sterols inhibiting different stages of SCAP-SREBP2 ER-to-Golgi translocation.

(B–G) LPS-primed BMDMs treated with different doses as indicated (B, C, and F) or 5 μM betulin (D, E, and G) for 30 min and then stimulated with ATP (B–F), nigericin (D, E, and G), MSU (D and E), or alum (D and E). Supernatants (SN) and cell extracts (Lysate) were analyzed by immunoblotting in (B) and (D), and supernatants were analyzed by ELISA for IL-1β and IL-18 release in (C) and (E). ASC oligomerization in cross-linked cytosolic pellets was analyzed by immunoblotting in (F), and representative immunofluorescence images and quantification of ASC speck formation are shown in (G). Scale bars, 200 μm (panel) and 20 μm (inset).

(legend continued on next page)

nigericin-induced caspase-1 maturation, IL-1β production, ASC oligomerization, and ASC-speck formation (Figures 2L, 2M, S2E, and S2F). Although cholesterol crystal has been shown to promote inflammasome activation and atherogenesis (Duewell et al., 2010; Sheedy et al., 2013), under physiological conditions, the ER contains a delicate feedback system that senses the excess cholesterol to inactivate SCAP-SREBP2 translocation and thus maintains the intracellular cholesterol within narrow limits (Goldstein et al., 2006; Radhakrishnan et al., 2008; Spann and Glass, 2013). As predicted, acute treatment with 20–60 μg/mL methyl-β-cyclodextrin (MCD)-cholesterol during activation stage of the NLRP3 inflammasome, concentrations typically used to inhibit SCAP-SREBP2 ER-to-Golgi translocation, clearly suppressed, rather than promoted, NLRP3 inflammasome activation in a dose-dependent manner (Figures 2N and 2O). Moreover, 60 μg/mL cholesterol did not directly activate the NLRP3 inflammasome in LPS-primed BMDMs as a danger signal like crystalline cholesterol (Figures 2N and 2O). Importantly, this inhibitory effect of cholesterol on NLRP3 inflammasome activation was prompt (Figure S2G), which is in line with the report that MCD-cholesterol is transferred rapidly from the plasma membrane to the ER by vesicular or non-vesicular carriers (Prinz, 2007). Furthermore, we also examined this regulatory effect of cholesterol on NLRP3 inflammasome with liposomal-cholesterol and obtained similar results (Figure S2H).

SCAP-SREBP2 plays a well-defined role in the transcriptional regulation of enzymes involved in the cholesterol-biosynthetic mevalonate pathway. However, consistent with the previous studies showing that blockade of the mevalonate pathway by statins enhances NLRP3 inflammasome activation (Próchnicki and Latz, 2017; Spann and Glass, 2013), NB-598 targeting downstream squalene epoxidase also slightly increased IL-1β production (Figures S2I and S2J). Taken together, our results suggest a role of SCAP-SREBP2 ER-to-Golgi translocation in activation of the NLRP3 inflammasome.

SCAP-SREBP2 Complex Is Required for Optimal NLRP3 Inflammasome Activation

We next adopted multiple genetic strategies to investigate the role of SCAP-SREBP2 in NLRP3 inflammasome activation. First, silencing of *Scap* (encoding SCAP) or *Srebf2* (encoding SREBP2) by small-interfering RNAs (siRNAs) blocked optimal NLRP3 inflammasome activation without affecting TNF-α production in peritoneal macrophages (Figures 3A and 3B). Second, we generated J774.1 and THP1 macrophages stably expressing shRNAs targeting *Scap* and *SREBF2*, respectively. Similarly, J774.1-SCAP-shRNA and THP1-SREBP2-shRNA macrophages showed greatly impaired NLRP3 inflammasome activity (Figures S3A–S3E). In contrast, TNF-α production and NLRC4 inflammasome activation remained unaffected in these cells (Figures S3F–S3H). In line with a previous study showing that SCAP deficiency in BMDMs had limited effect on total amounts of lipids including cholesterol (York et al., 2015), these stable *Scap*-silenced macrophages showed minimally affected cellular cholesterol amounts (Figure S3I), suggesting that SCAP may control NLRP3 inflammasome activation without affecting cellular cholesterol amounts.

We also confirmed these observations with macrophage-specific deletion of SCAP using the *Lyz2-cre* model (*Lyz2-cre-Scap*$^{f/f}$). As expected, BMDMs from *Lyz2-cre-Scap*$^{f/f}$ mice had impaired NLRP3 inflammasome activation triggered by different NLRP3 agonists compared with control mice (Figures 3C–3E). Moreover, compared with wild-type mice, the remaining NLRP3 inflammasome activity in BMDMs from *Lyz2-cre-Scap*$^{f/f}$ mice caused by the residual SCAP expression showed a similar kinetic response upon ATP stimulation (Figure 3D), suggesting that SCAP deficiency may not affect response sensitivity of the NLRP3 inflammasome. In contrast, TNF-α production was unaffected in the absence of SCAP (Figure 3E). To further examine whether any potential changes in cholesterol homeostasis contribute to this suppressed NLRP3 activity caused by SCAP deficiency, we supplemented different concentrations of MCD-cholesterol in these macrophages. In line with the results that cholesterol suppressed NLRP3 inflammasome activation (Figures 2O and S2F), supplementation of MCD-cholesterol suppressed, rather than restored, IL-1β production with a similar kinetic pattern in both wild-type and SCAP-deficient BMDMs (Figure 3F). These results together suggest that SCAP may play a direct role in NLRP3 inflammasome activation rather than change cholesterol homeostasis.

Previous studies have demonstrated that overexpression of SCAP or SREBP2 leads to spontaneous SCAP-SREBP2 ER-to-Golgi translocation (Sakai et al., 1998). Consistently, stably transfected THP1 macrophages overexpressing SCAP or SREBP2 showed increased NLRP3 inflammasome activity (Figures 3G–3J). A similar result was also obtained in immortalized BMDMs stably overexpressing SCAP (Figure S3J). To further confirm that this promoting effect of SCAP on the NLRP3 inflammasome occurs at the activation stage, we reconstituted NLRP3 inflammasomes in HEK293T cells without expression of pro-IL-1β. Notably, overexpression of SCAP promoted nigericin-induced caspase-1 maturation (Figure 3K). Besides overexpressing their components, we further assessed the effect of SCAP-SREBP2 on the NLRP3 inflammasome by using a "SCAP-SREBP2 activating medium" which constitutively transports SCAP-SREBP2 from the ER to the Golgi apparatus caused by the sterol depletion (Goldstein et al., 2006). We found that this medium enhanced nigericin-induced caspase-1 maturation as well as IL-1β and IL-18 secretion compared with the control medium (Figures 3L and 3M), while the production of TNF-α was less affected (Figure 3M). More importantly, without an NLRP3 agonist, SCAP-SREBP2 activating medium alone promoted the maturation of IL-1β (Figures 3M and S3K). In addition, we induced acute SCAP-SREBP2 ER-to-Golgi translocation by

(H and I) LPS-primed BMDMs treated with 5 μM betulin for 30 min and then stimulated with ATP, poly (dA:dT), or *Salmonella typhimurium* (*Salmonella*) infection. Supernatants (SN) and cell extracts (Lysate) were analyzed by immunoblotting (H). IL-1β release in supernatants was analyzed by ELISA (I).

(J–O) LPS-primed BMDMs treated with different doses of fatostatin (J and K), 25-HC (L and M), or MCD-cholesterol (N and O) as indicated for 30 min (J, K, N, and O), or 8 hr (L and M), and then stimulated with ATP. Supernatants (SN) and cell extracts (Lysate) were analyzed by immunoblotting (J, L, and N). Supernatants were analyzed by ELISA for IL-1β and IL-18 release (K, M, and O).

*p < 0.05, **p < 0.01, ***p < 0.001. Values are mean ± SD. Data are representative of three independent experiments. See also Figure S2.

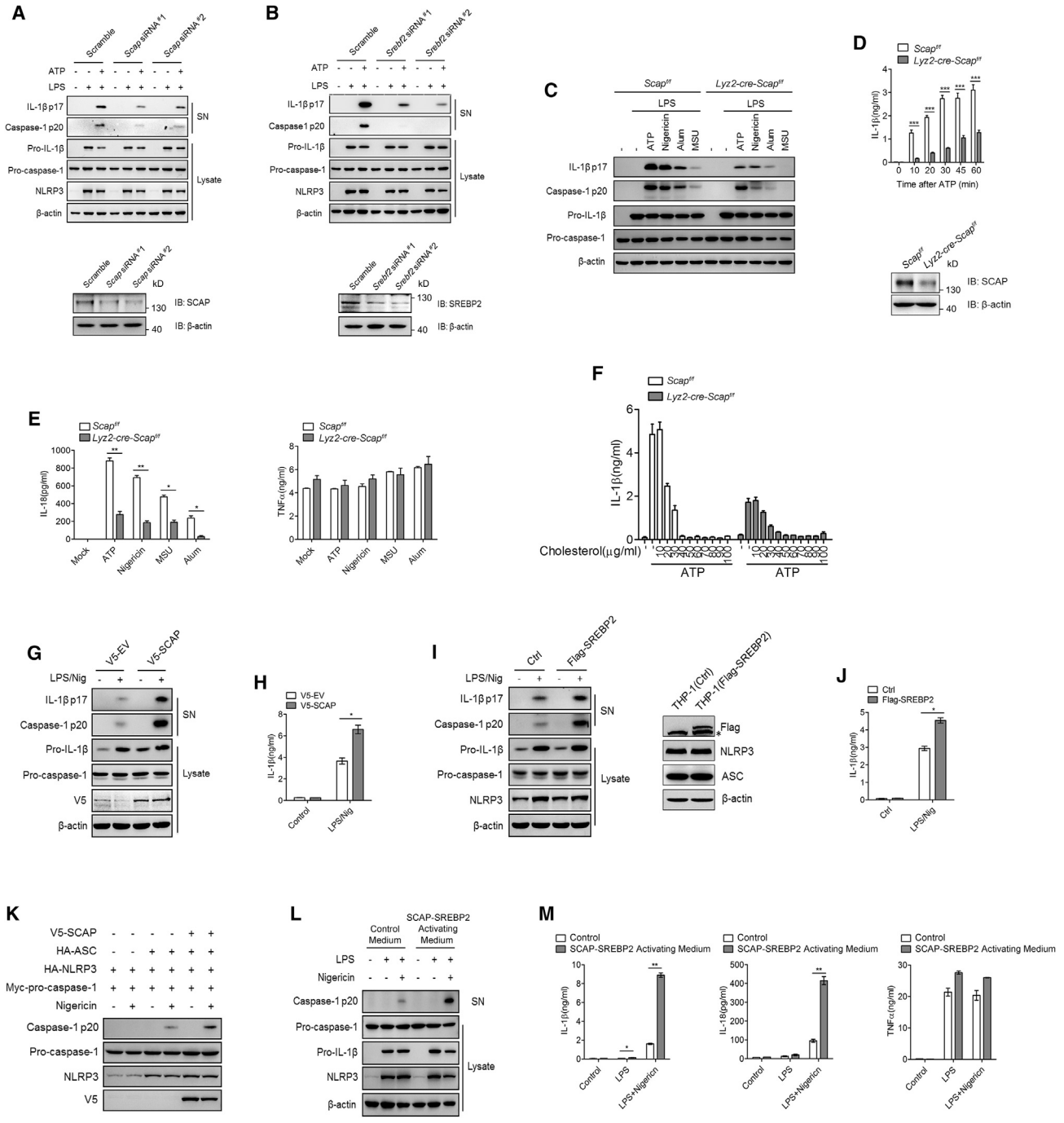

Figure 3. SCAP-SREBP2 Complex Is Required for Optimal NLRP3 Inflammasome Activation

(A and B) Immunoblotting of supernatants (SN) and cell extracts (Lysate) from LPS-primed peritoneal macrophages transfected with scrambled control (A and B), *Scap*-specific (A), or *Srebf2*-specific siRNAs (B) and stimulated with ATP.

(C–E) Immunoblotting (C) and ELISA (D and E) of supernatants (SN) and cell extracts (Lysate) from LPS-primed BMDMs from control and *Lyz2-cre-Scap*$^{f/f}$ mice stimulated with ATP, nigericin, MSU, or alum.

(F) ELISA of supernatants from LPS-primed BMDMs from control and *Lyz2-cre-Scap*$^{f/f}$ mice stimulated with ATP in the absence or presence of different concentrations of MCD-cholesterol as indicated.

(G–J) Immunoblotting (G and I) and ELISA (H and J) of supernatants (SN) and cell extracts (Lysate) from LPS-primed THP1-V5-SCAP (G and H) and THP1-Flag-SREBP2 (I and J) macrophages stably expressing V5-SCAP and Flag-SREBP2 and stimulated with nigericin.

(K) Immunoblotting for extracts of HEK293T cells reconstituted by transfection with HA-ASC, NLRP3, Myc-pro-caspase-1, and V5-SACP stimulated with nigericin.

(legend continued on next page)

sterol extraction with methyl-β-cyclodextrin (Goldstein et al., 2006; Gurcel et al., 2006). As expected, ATP-induced IL-1β production was augmented (Figure S3L). Similarly, MCD alone spontaneously triggered the maturation of IL-1β in LPS-primed macrophages, and this effect was impeded by inhibiting SCAP-SREBP2 translocation with 25-HC (Figure S3L). These results together suggest that enforced cholesterol biosynthetic signaling in macrophages promotes activation of the NLRP3 inflammasome.

Optimal NLRP3 Inflammasome Activation Requires Golgi S1P- but Not S2P-Mediated SREBP2 Cleavage

To address the role of S1P- and S2P-mediated two-step cleavage in NLRP3 inflammasome activation, we first silenced the expression of S1P and S2P with siRNAs targeting *Mbtps1* (encoding S1P) and *Mbtps2* (encoding S2P) in peritoneal macrophages (Figures S4A–S4C). Our results revealed that specific siRNA-mediated reduction of S1P but not S2P resulted in marked suppression of NLRP3 inflammasome activation (Figures 4A–4D, S4D, and S4E). These results are in line with the report that the release of SCAP from the Golgi depends on the cleavage of SREBP protein by S1P but not S2P (Shao and Espenshade, 2014), suggesting a requirement of SCAP release from the Golgi for optimal NLRP3 inflammasome activation. We next generated mice deficient in S1P in macrophages (*Lyz2-cre-Mbtps1*$^{f/f}$) and found that the S1P-deficient BMDMs had greatly impaired NLRP3 inflammasome activity triggered by different NLRP3 agonists (Figures 4E, 4F, and S4F). Consistently, supplementation of different concentrations of cholesterol did not restore the decreased NLRP3 inflammasome activity in S1P-deficient BMDMs, but rather suppressed its residual NLRP3 inflammasome activity in a similar kinetic pattern to wild-type BMDMs (Figure 4G). In addition, we investigated the involvement of S1P in NLRP3 inflammasome activation using PF-429242 and AEBSF, two S1P inhibitors that do not affect S2P activity (Okada et al., 2003; Shao and Espenshade, 2014). Our results revealed that acute treatment of either AEBSF or PF-429242 greatly suppressed the NLRP3 inflammasome activity (Figures 4H–4J), without affecting cellular cholesterol amounts and viability (Figures S2A and S2B). Brefeldin A (BFA), which causes the Golgi to collapse into the ER and results in constitutive processing of SREBP2 in the ER by relocating S1P to the ER (DeBose-Boyd et al., 1999), spontaneously induced IL-1β secretion without an NLRP3 agonist (Figures 4K and 4L). Importantly, this secretion was suppressed by S1P inhibition with AEBSF (Figures 4K and 4L), suggesting that enforced S1P-mediated cleavage of SREBP2 promoted NLRP3 inflammasome activation. In contrast, the production of TNF-α was not affected in these experiments (Figures 4K and 4L). In addition to BFA, we retrovirally transduced *Lyz2-cre-Scap*$^{f/f}$ BMDMs with a mutant form of S1P that contains an ER retention and retrieval signal, Lys-Asp-Glu-Leu (KDEL). This also causes relocation of S1P from the Golgi to the ER and bypasses the SCAP requirement for SREBP2 cleavage (DeBose-Boyd et al., 1999). Compared with the empty vector, S1P-KDEL enhanced NLRP3 inflammasome activation but not TNF-α production in *Lyz2-cre-Scap*$^{f/f}$ BMDMs, while the inactive S1P-KDEL-S414A mutant had no effect (Figures 4M and S4G). Together, these results suggest that S1P-mediated SREBP2 cleavage promotes NLRP3 inflammasome activation.

NLRP3 Associates with SCAP and SREBP2 via the NACHT Domain

The requirement of SCAP-SREBP2 for optimal NLRP3 inflammasome activation prompted us to investigate the possibility that NLRP3 associates with this complex. Co-immunoprecipitation analysis in LPS-primed BMDMs and THP1 macrophages stably expressing V5-SCAP revealed the association of NLRP3 with SCAP upon ATP and nigericin stimulation (Figures 5A and 5B). Similarly, NLRP3 also associated with SREBP2 in LPS-primed BMDMs and THP1 macrophages stably expressing Flag-SREBP2, and this was further enhanced by stimulation with an NLRP3 agonist (Figures 5C and 5D). To further confirm these interactions, we performed GST pull-down assay and found the direct interaction of NLRP3 with either SCAP or SREBP2 (Figures 5E and 5F). To further delineate the association of NLRP3 with the SCAP-SREBP2 complex, we introduced various truncated mutants of these proteins according to their domain structures into HEK293T cells (Figure 5G). As predicted, NLRP3 associated with the SCAP WD40-repeat domain but not the N-terminal transmembrane domain, mainly through its NACHT domain (Figures 5H, 5I, S5A, and S5B). In addition, the NLRP3 NACHT domain and the SREBP2 C-terminal regulatory domain were mainly required for the association between NLRP3 and SREBP2 (Figures 5J, 5K, S5C, and S5D). These results presented thus far support a scenario in which NLRP3 associates with both SCAP and SREBP2, so we hypothesized that a ternary complex might be formed with these three proteins. To test this hypothesis, we performed co-immunoprecipitation experiments in HEK293T cells transfected with V5-SCAP, HA-NLRP3, and Flag-SREBP2. Immunoprecipitation of SREBP2 pulled down both SCAP and NLRP3, while immunoprecipitation of SCAP pulled down both NLRP3 and SREBP2 (Figure 5L). Furthermore, we performed a two-step co-immunoprecipitation assay in these cells. As expected, NLRP3 was present in the final immunoprecipitate but not in the control samples (Figure 5M). In contrast, SCAP and SREBP2 did not associate with other essential components of the NLRP3 inflammasome, including NEK7 and ASC (Figures S5E and S5F). Taken together, our results suggest that SCAP-SREBP2 promotes NLRP3 inflammasome activation by forming a ternary complex with NLRP3.

NLRP3 Associates with SCAP for Its Golgi Translocation during NLRP3 Inflammasome Activation

Considering its well-established escort function and association with NLRP3, we hypothesized that SCAP might also be

(L and M) Immunoblotting (L) and ELISA (M) of supernatants (SN) and cell extracts (Lysate) from BMDMs cultured for 16 hr in control medium or SCAP-SREBP2 activating medium with 10% lipoprotein-deficient serum (LPDS), 10 μM lovastatin, and 50 μM mevalonate primed with LPS for 4 hr, and then stimulated with nigericin.

*p < 0.05, **p < 0.01, ***p < 0.001. Values are mean ± SD. Data are representative of three independent experiments. See also Figure S3.

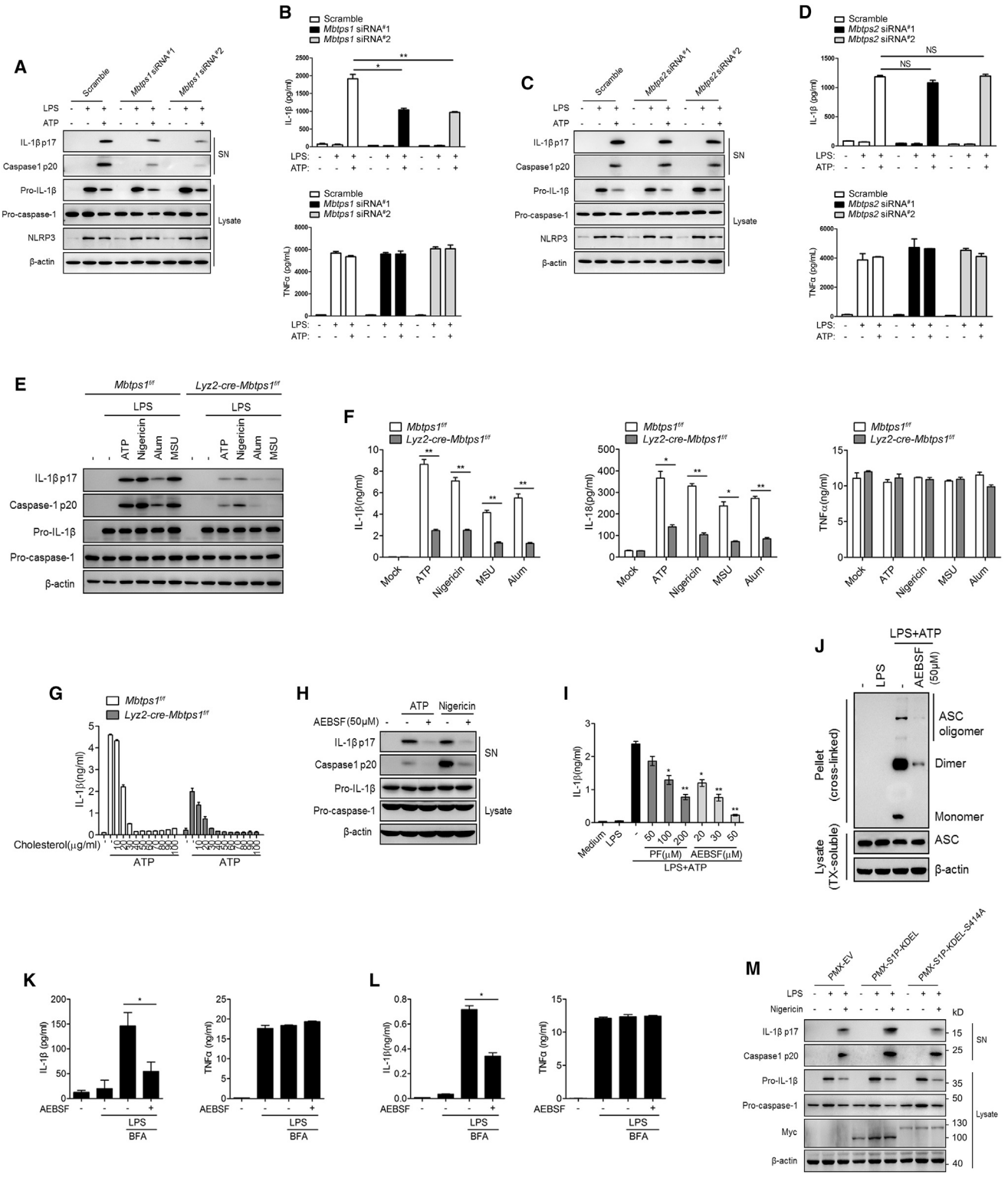

Figure 4. Optimal NLRP3 Inflammasome Activation Requires Golgi S1P- but not S2P-Mediated SREBP2 Cleavage

(A–D) Immunoblotting (A and C) and ELISA (B and D) of supernatants (SN) and cell extracts (Lysate) from LPS-primed peritoneal macrophages transfected with scrambled control (A–D), *Mbtps1*-specific (A and B), or *Mbtps2*-specific siRNAs (C and D) and stimulated with ATP.

(E and F) Immunoblotting (E) and ELISA (F) of supernatants (SN) and cell extracts (Lysate) from LPS-primed BMDMs from control and *Lyz2-cre-Mbtps1*$^{f/f}$ mice stimulated with ATP, nigericin, alum, or MSU.

(legend continued on next page)

involved in the translocation of NLRP3 required for its optimal activation (Próchnicki and Latz, 2017; Rathinam and Fitzgerald, 2016). In LPS-primed BMDMs, NLRP3 was partially co-localized with SCAP or SREBP2 in the perinuclear region, and this was markedly enhanced by ATP stimulation (Figures 6A and 6B). Furthermore, we performed *in situ* proximity ligation assays, which are suitable for quantitative studies of the spatial proximity of two molecules. In line with the confocal analysis, we found that LPS caused spatial approximation of NLRP3 to SCAP or SREBP2 in BMDMs, and this was markedly enhanced by ATP stimulation (Figures 6C and 6D). HEK293T cells expressing NLRP3 with more physiological amounts can be used to investigate the subcellular translocation of NLRP3 during inflammasome activation (Figure S6A; Subramanian et al., 2013). As found in BMDMs, a small portion of resting NLRP3 was in close proximity to SCAP in the perinuclear region, which was markedly promoted upon nigericin stimulation (Figure S6B).

The Golgi serves as a critical platform for SREBP2 processing, but its contribution to the NLRP3 inflammasome remains largely unknown. To examine more precisely the involvement of NLRP3 translocation in the dynamics of Golgi and mitochondria during inflammasome activation, we performed super-resolution and 3D-structured illumination microscopy (SIM) imaging in BMDMs. We observed that ATP stimulation re-localized NLRP3 to regions very close to the Golgi membranes (Figure 6E; Videos S2 and S3). In the resting state, the mitochondria were string-like in shape (Figure 6E; Video S1). In contrast, dot-like mitochondrial clustering, representing damaged mitochondria and thought to provide several factors necessary for NLRP3 activation (Próchnicki and Latz, 2017; Zhou et al., 2011), was observed adjacent to the Golgi membranes with NLRP3 (Figure 6E; Videos S2 and S3), in line with a very recent study showing that activation of the NLRP3 inflammasome induces mitochondrial clustering around the Golgi (Zhang et al., 2017). To confirm these observations, we studied subcellular fractions from THP1-V5-SCAP macrophages. Notably, NLRP3 was substantially detected in the Golgi fraction (Figure 6F), and more importantly, SCAP and NLRP3 were both detected in the mitochondrial fraction in a roughly similar manner upon nigericin stimulation (Figure 6G). Last, using super-resolution and 3D-SIM, we observed that a portion of NLRP3 was localized close to both SCAP and the COPII protein Sec23A (Figure S6C), suggesting that the COPII-coated vesicles may also be used by SCAP for NLRP3 transport during inflammasome activation. Altogether, we hypothesized that the interface between Golgi and mitochondrial clustering may provide a platform for NLRP3 inflammasome activation.

SCAP-SREBP2 Promotes NLRP3 Inflammasome Activation *In Vivo*

We finally set out to determine whether SCAP-SREBP2 promotes NLRP3 inflammasome activation *in vivo*. First, when challenged with LPS, *Lyz2-cre-Scap*$^{f/f}$ mice showed significantly reduced serum IL-1β and IL-18 but unaffected TNF-α production (Figure 7A). Moreover, SCAP deficiency in macrophages significantly increased the survival of mice challenged with LPS (Figure S7A). Second, betulin or fatostatin treatment significantly reduced LPS-induced serum IL-1β and IL-18 production, similar to the reduction seen in *Lyz2-cre-Scap*$^{f/f}$ mice (Figures 7B and 7C). Importantly, there was little additional decrease in IL-1β and IL-18 production when we treated *Lyz2-cre-Scap*$^{f/f}$ mice with betulin or fatostatin, suggesting that SCAP-SREBP2 is the main target of betulin or fatostatin in this sepsis model (Figures 7B and 7C). In contrast, TNF-α production was little affected (Figures 7B and 7C). Third, in agreement with the results *in vitro*, 25-HC administration resulted in a substantial decrease of LPS-induced serum IL-1β but not TNF-α (Figure 7D). Similarly, this inhibitory effect of 25-HC was clearly blunted in *Lyz2-cre-Scap*$^{f/f}$ mice (Figure 7D).

We next addressed the role of SCAP-SREBP2 in NLRP3 inflammasome activation *in vivo* using a model of alum-induced peritonitis. As expected, IL-1β secretion in the lavage fluid was impaired in *Lyz2-cre-Scap*$^{f/f}$ mice. Moreover, the peritoneal exudate cells and neutrophils recruited upon alum challenge were significantly fewer in these mice (Figure 7E). Consistently, 25-HC treatment also suppressed the alum-induced peritonitis *in vivo* (Figure S7B), suggesting an immunomodulatory effect of this endogenous sterol during inflammatory responses *in vivo*, at least in the models of sepsis and peritonitis we explored.

Statins are widely used for lowering cholesterol by targeting HMG CoA reductase. However, their potent action of blocking *de novo* cholesterol synthesis also enhances SCAP-SREBP2 activation *in vivo* (Matsuda et al., 2001; Spann and Glass, 2013). Our results revealed that both in the sepsis and peritonitis models, mice fed a diet supplemented with 0.2% lovastatin for 4 days showed markedly higher IL-1β production than control mice (Figures 7F and 7G), while the TNF-α production remained unaffected (Figure 7F). However, lovastatin administration suppressed, rather than promoting, IL-1β production in *Lyz2-cre-Scap*$^{f/f}$ mice, suggesting that the complex effects of statins on IL-1β production depend on the activity of SCAP-SREBP2 (Figure S7C). In addition, this promoting effect of lovastatin on IL-1β production was recapitulated in human peripheral blood mononuclear cells (PBMCs). Importantly, betulin and fatostatin suppressed this effect, suggesting a potential promoting action of statins on IL-1β production via SCAP-SREBP2 activation (Figure S7D).

(G) ELISA of supernatants from LPS-primed BMDMs from control and *Lyz2-cre-Mbtps1*$^{f/f}$ mice stimulated with ATP in the absence or presence of different concentrations of MCD-cholesterol as indicated.

(H–J) LPS-primed BMDMs were treated with AEBSF or PF-429242 as indicated for 1 hr, and then stimulated with ATP or nigericin. Supernatants (SN) and cell extracts (Lysate) were analyzed by immunoblotting (H) and ELISA (I). ASC oligomerization in cross-linked cytosolic pellets was analyzed by immunoblotting (J).

(K and L) ELISA of supernatants from LPS-primed BMDMs (K) and THP1 macrophages (L) treated with 0.5 μg/mL BFA for 6 hr in the absence or presence of AEBSF.

(M) Immunoblotting of supernatants (SN) and cell extracts (Lysate) from LPS-primed *Lyz2-cre-Scap*$^{f/f}$ BMDMs retrovirally transduced with PMX empty vector, PMX-S1P-KDEL, or PMX-S1P-KDEL-S414A stimulated with nigericin.

*$p < 0.05$, **$p < 0.01$, NS, $p > 0.5$. Values are mean ± SD. Data are representative of three independent experiments. See also Figure S4.

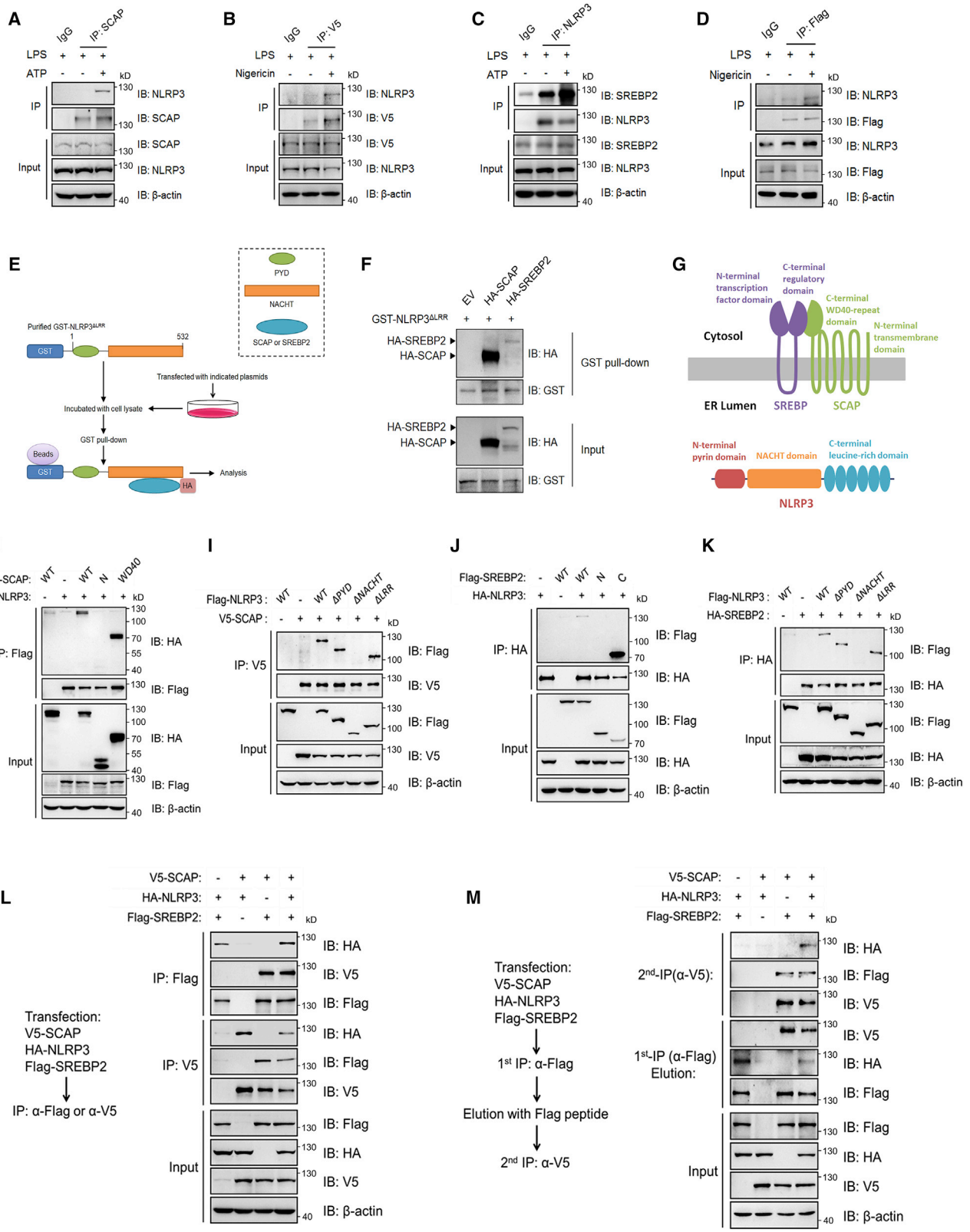

(legend on next page)

Last, gain-of-function mutations in the *Nlrp3* gene result in its activation or predisposition for activation and are associated with the cryopyrin-associated periodic fever syndromes (CAPS) (Masters et al., 2009). We retrovirally transduced the BMDMs from *Nlrp3*^{A350VneoR} mice (corresponding to CAPS patient NLRP3^{A352V}) with Cre to induce NLRP3^{A350V} activation (Brydges et al., 2009). We found that this NLRP3^{A350V}-mediated IL-1β production was greatly suppressed by betulin, fatostatin, or AEBSF (Figure 7H). Similarly, these inhibitors suppressed another CAPS-associated NLRP3^{R258W}-mediated IL-1β production (Figure S7E). Collectively, these results indicate that SCAP-SREBP2 activation promotes NLRP3 inflammasome activity *in vivo* and suggest SCAP-SREBP2 as a potential target for NLRP3-related diseases.

DISCUSSION

In this study, we established a previously unknown and unexpected role for the SCAP-SREBP2 complex in pro-inflammatory macrophages as an important signaling hub integrating cholesterol metabolism and innate immunity. In line with our result that enforced activation of cholesterol biosynthetic signaling promoted spontaneous NLRP3 inflammasome activation, a central facet of the type I interferon-mediated suppressive effect on immunity is downregulation of inflammasome activity (Guarda et al., 2011) and its signaling is spontaneously activated by limiting cholesterol synthetic flux (York et al., 2015). Thus, these results suggested that cholesterol synthetic flux in immune cells may be part of the metabolic-inflammatory circuit to ensure that any changes in the activity of one can be sensed by the other.

Although cholesterol biosynthetic signaling is coupled to NLRP3 inflammasome activation, the promoting effect of SCAP-SREBP2 on NLRP3 inflammasome activation was independent of the transcriptional activity of n-SREBP2 controlling the cholesterol biosynthetic genes involved in the mevalonate pathway. Instead, our study indicates that statins potentially promote NLRP3 inflammasome activation and IL-1β production via enhancing SCAP-SREBP2 activation. Statins are widely used to lower cholesterol in the blood, but they have also been associated with increased risk of additional-onset diabetes and myopathy (Sattar et al., 2010). Therefore, it will be worthwhile to examine their effects on inflammasome activation in human subjects; this might foster additional therapeutic and diagnostic strategies for statin-induced risk of disease.

There are discrepancies in the roles of cholesterol and its related metabolites in NLRP3 inflammasome activation. Besides the cholesterol crystals (Duewell et al., 2010), non-crystalline cholesterol at high concentrations is also reported to directly trigger activation of the inflammasomes, possibly by impairing mitochondrial function (Dang et al., 2017; Youm et al., 2012). In contrast, we found that cholesterol and 25-HC had potent inhibitory effects on activation stage of the NLRP3 inflammasome. In addition, MCD-induced cholesterol depletion promoted NLRP3 inflammasome activation, in line with the report that reduced plasma membrane cholesterol enhances NLRP3 inflammasome activation (Lordén et al., 2017). Moreover, two recent studies have reported that cholesterol 25-hydroxylase (Ch25h) has an inhibitory effect on inflammasomes by synthesizing 25-HC from cholesterol (Dang et al., 2017; Reboldi et al., 2014). Of note, Ch25h is induced in macrophages by type I interferons downstream of Toll-like receptor 3 (TLR3) or TLR4 activation (Cyster et al., 2014), suggesting that this immunomodulatory effect of 25-HC might occur in a later phase of the inflammatory responses. However, a recent study also reported that 25-HC activates the NLRP3 inflammasome, leading to cerebral inflammation (Jang et al., 2016). Taken together, these results suggest that, depending on the cell type and cellular sterol homeostasis (e.g., amount, type, crystal formation, and intracellular distribution) in different phases of inflammatory responses, cholesterol and/or sterols may directly or indirectly (for example, converted to 25-HC) exert either a positive or a negative influence on NLRP3 activation.

Our results strongly support the idea that SCAP-SREBP2 promotes NLRP3 inflammasome activation mainly in a direct manner without affecting cholesterol homeostasis. However, this raises the question of the physiological purpose of the increased cholesterol biosynthetic signaling during NLRP3 inflammasome activation, which was not addressed in this study. Recently, an increasing body of evidence has suggested that the inflammasome-mediated cytokine maturation and pyroptosis are not tightly coupled (Gaidt et al., 2016; Yan et al., 2013; Zanoni et al., 2016). A very recent study identified a non-pyroptotic function of GSDMD for IL-1β release in living macrophages with a "hyperactivated" status between "activated" and "pyroptotic" status (Evavold et al., 2018). The pyroptosis offers the benefit of a

Figure 5. NLRP3 Associates with SCAP and SREBP2 via the NACHT Domain

(A–D) Immunoblotting of immunoprecipitation with anti-SACP (A), anti-V5 (B), anti-NLRP3 (C), and anti-Flag (D) from LPS-primed BMDMs (A and C), THP1-V5-SCAP macrophages stably expressing V5-SCAP (B), or THP1-Flag-SREBP2 macrophages stably expressing Flag-SREBP2 (D) stimulated with ATP (A and C) or nigericin (B and D) for 30 min.

(E) Schematic of GST pull-down assay for the detection of NLRP3 interaction with SCAP or SREBP2.

(F) HEK293T cells were transfected with HA-SCAP or HA-SREBP2. Cell lysates were incubated with purified GST-NLRP3 ΔLRR for 2 hr. HA-SCAP and HA-SREBP2 bound with GST-NLRP3 ΔLRR were pulled down by glutathione beads and subjected to immunoblot analysis.

(G) Schematic of domain structures of SCAP, SREBP2, and NLRP3.

(H and I) Immunoblotting of immunoprecipitation with anti-Flag (H) or anti-V5 (I) in HEK293T cells transfected with the HA-SCAP N terminus (N) or WD40 domain and Flag-NLRP3 ΔPYD, ΔNACHT, or ΔLRR.

(J) HEK293T cells transfected with Flag-SREBP2 N terminus (N) or C terminus (C) and HA-NLRP3 immunoprecipitated with anti-HA for subsequent immunoblotting analysis.

(K) HEK293T cells transfected with Flag-NLRP3 ΔPYD, ΔNACHT, or ΔLRR and HA-SREBP2 immunoprecipitated with anti-HA for subsequent immunoblotting analysis.

(L and M) HEK293T cells were transfected with V5-SCAP, HA-NLRP3, and Flag-SREBP2. Flag immunoprecipitates and V5 immunoprecipitates were analyzed by immunoblotting as outlined (L). A two-step co-immunoprecipitation assay was performed with the cell lysates as outlined (M).

Data are representative of three independent experiments. See also Figure S5.

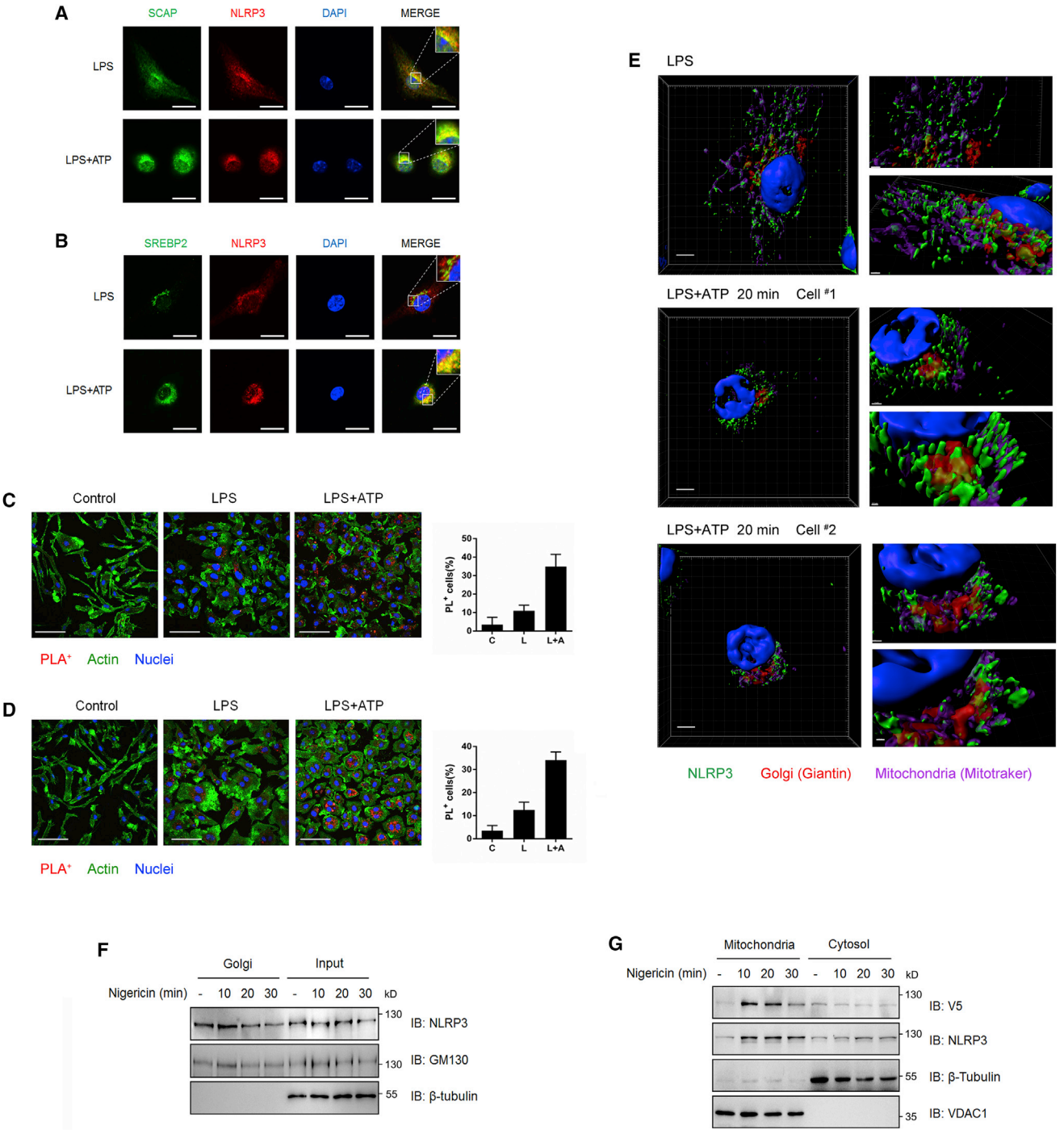

Figure 6. NLRP3 Associates with SCAP for Its Golgi Translocation during NLRP3 Inflammasome Activation

(A and B) BMDMs analyzed for co-localization of NLRP3 with SCAP (A) or SREBP2 (B) by confocal microscopic imaging. Scale bars, 15 μm.

(C and D) BMDMs analyzed for the spatial approximation of NLRP3 to SCAP (C) or SREBP2 (D) by proximity ligation assay (PLA): red, proximity ligation-positive (PL^+) signals; green, actin filaments; blue, nuclei. Scale bars, 50 μm.

(E) Super-resolution and 3D-structured illumination microscopy (SIM) imaging in BMDMs stimulated as indicated with staining for NLRP3 (green), Golgi (red), and mitochondria (purple). Enlarged 3D images are shown on the right. Scale bars, LPS: 3 μm (left) and 1 μm (right); LPS+ATP 20 min: 3 μm (left), 1 μm (upper right), 0.5 μm (lower right).

(F) Immunoblotting of Golgi fractions and total cell lysates (input) from LPS-primed THP1 macrophages stimulated with nigericin as indicated.

(G) Immunoblotting of mitochondrial and cytosolic fractions in LPS-primed THP1-V5-SCAP macrophages stably expressing V5-SCAP stimulated with nigericin as indicated.

Data are representative of three independent experiments. See also Figure S6 and Videos S1, S2, and S3.

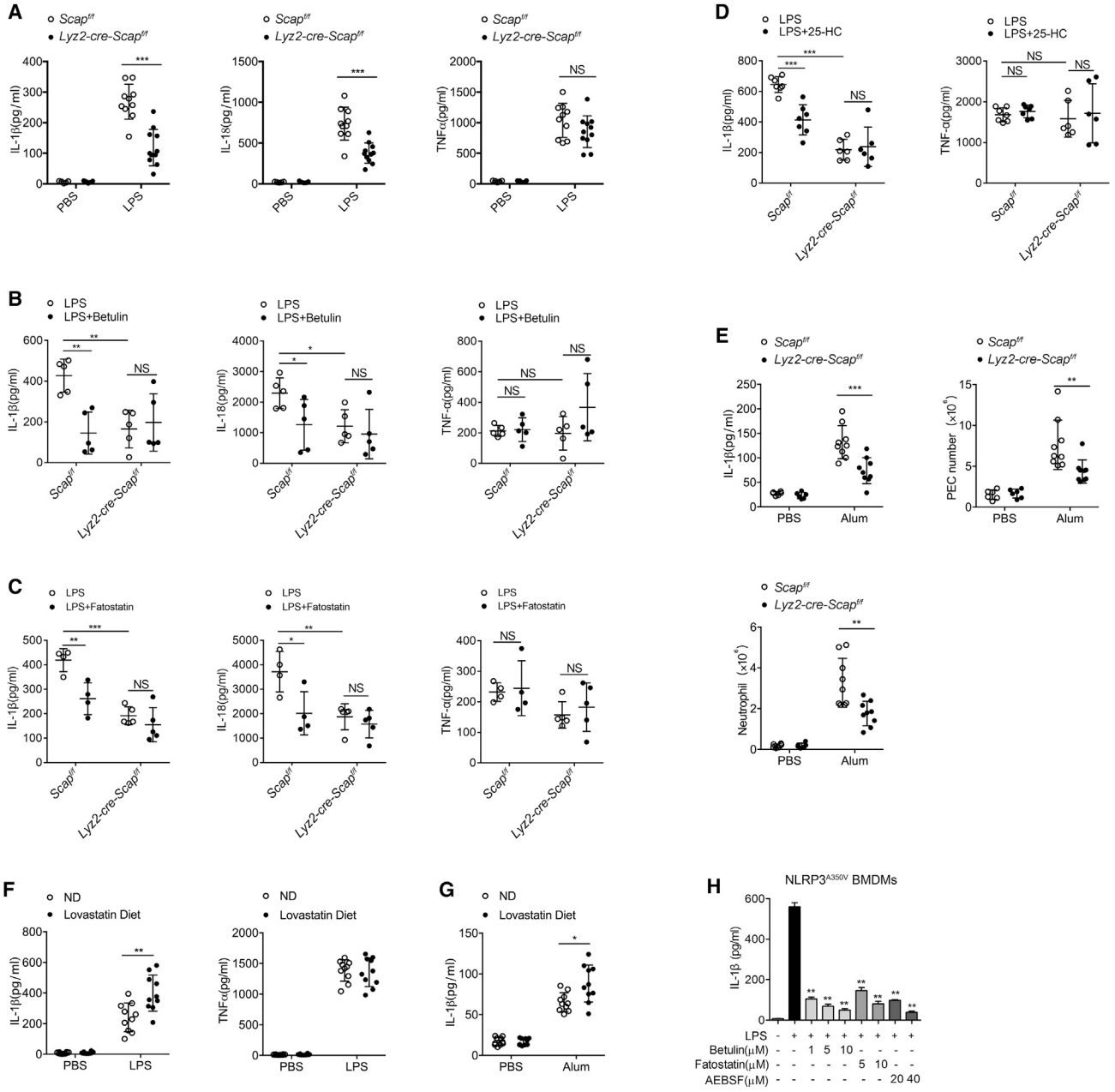

Figure 7. SCAP-SREBP2 Promotes NLRP3 Inflammasome Activation *In Vivo*

(A) ELISA of IL-1β, IL-18, and TNF-α in serum from control and *Lyz2-cre-Scap*$^{f/f}$ mice intraperitoneally injected with LPS (20 mg/kg body weight) for 4 hr (PBS: n = 5 mice/group; LPS: n = 10–11 mice/group).

(B–D) ELISA of IL-1β, IL-18, and TNF-α in serum from control and *Lyz2-cre-Scap*$^{f/f}$ mice intraperitoneally injected with LPS (20 mg/kg body weight) for 4 hr in the presence or absence of betulin (30 mg/kg body weight) (n = 5 mice/group) (B), fatostatin (20 mg/kg body weight) (n = 4–5 mice/group) (C), or 25-HC (50 mg/kg body weight) (n = 6–7 mice/group) (D).

(E) ELISA of IL-1β and flow cytometry analysis of peritoneal exudate cells and neutrophil numbers in the peritoneal cavity from control and *Lyz2-cre-Scap*$^{f/f}$ mice intraperitoneally injected with alum for 6 hr (PBS: n = 6 mice/group; alum: n = 9 mice/group).

(F) ELISA of IL-1β and TNF-α in serum from wild-type mice fed on a diet with or without 0.2% lovastatin (wt/wt) for 4 days and then intraperitoneally injected with LPS for 4 hr (20 mg/kg body weight) (n = 10 mice/group).

(G) ELISA of IL-1β in the peritoneal cavity of wild-type mice fed on a diet with or without 0.2% lovastatin (w/w) for 4 days and then intraperitoneally injected with alum for 6 hr (n = 10 mice/group).

(H) ELISA of supernatants from *Nlrp3*^{A350VneoR} BMDMs retrovirally transduced with PMX-Cre stimulated with LPS in the absence or presence of betulin, fatostatin, or AEBSF as indicated for 10 hr.

*p < 0.05, **p < 0.01, ***p < 0.001, NS, p > 0.5. Values are mean ± SD. Data are representative of two or three independent experiments. See also Figure S7.

massive inflammatory response. However, the cost of pyroptosis is the loss of any necessary immunomodulatory activities. We therefore propose that the "activated" macrophages may have a mechanism that senses the severity of a threat to determine whether cell death is obligatory for defense. Otherwise, if secreted cytokines are capable of relieving the threat, SCAP-SREBP complex-mediated lipogenesis could preserve the integrity of the plasma membrane to promote cell survival. In line with this hypothesis, bacterial pore-forming toxins activate the inflammasome to promote caspase-1 activation in mammalian fibroblasts, which further acts on an as-yet-unknown intermediate target to induce SREBP processing for cell survival (Gurcel et al., 2006).

Our results revealed that the interface between Golgi and mitochondrial clustering may function as an important platform for NLRP3 inflammasome activation, which is in line with a very recent study reporting a similar observation (Zhang et al., 2017). More importantly, Golgi collapse caused by brefeldin A blocked nigericin-induced and virus-induced NLRP3 inflammasome activation, suggesting an essential role of the intact Golgi apparatus in NLRP3 inflammasome activation (Ichinohe et al., 2010; Triantafilou et al., 2013; Zhang et al., 2017). Of note, brefeldin A also blocks anterograde transport and translocates Golgi proteins, including S1P, back to the ER. We found that brefeldin A alone served as an NLRP3 agonist, and this was suppressed by S1P inhibition. These results may explain why the brefeldin A-induced NLRP3 inflammasome activation seems to be independent of ER stress and unfolded protein response (Bronner et al., 2015; Menu et al., 2012).

In conclusion, the studies described here provide mechanistic insights into how SCAP-SREBP2 complex-mediated cholesterol biosynthetic signaling engages optimal activation of the NLRP3 inflammasome and advances our understanding of the metabolic-inflammatory circuit in pro-inflammatory macrophages.

STAR★METHODS

Detailed methods are provided in the online version of this paper and include the following:

- KEY RESOURCES TABLE
- CONTACT REAGENTS AND RESOURCE SHARING
- EXPERIMENTAL MODEL AND SUBJECT DETAILS
  - Mice
  - Cells
  - Reagents
- METHOD DETAILS
  - Reconstitution of NLRP3 Inflammasome in HEK293T cells
  - Transfection and Co-Immunoprecipitation
  - ASC Oligomerization and ASC Speck Formation
  - Small-interfering RNA Transfection
  - Cellular Fractionation
  - Quantitative PCR
  - Total Cholesterol Assessment
  - Immunofluorescence Staining and Confocal Microscopy
  - Super-resolution Microscopy and Structured Illumination Microscopy
  - Proximity Ligation Assay
  - Virus Transduction of THP1 and J774.1 Macrophages
  - ELISA
  - Liposomal-Cholesterol Preparation
  - Sterol-Depletion Experiments
  - *In Vivo* LPS Challenge
  - Alum-Induced Peritonitis
- QUANTIFICATION AND STATISTICAL ANALYSIS

SUPPLEMENTAL INFORMATION

Supplemental Information includes seven figures and three videos and can be found with this article online at https://doi.org/10.1016/j.immuni.2018.08.021.

ACKNOWLEDGMENTS

We thank Dr. Feng Shao (National Institute of Biological Sciences) for providing immortalized mouse macrophages and Dr. Tao Li (National Center of Biomedical Analysis) for providing plasmid of GST-NLRP3 ΔLRR. We thank Dr. I.C. Bruce for reading the manuscript. This work was supported by the National Natural Science Foundation of China (81730047, 31522020, 31670926), the National Key Research and Development Program of China (2018YFC1105203, 2016YFC1100204), and Fundamental Research Funds for the Central Universities (2015XZZX004-31).

AUTHOR CONTRIBUTIONS

C.G., Z.C., D.J., T.X., W.Y., Z.W., L.Z., Q.L., X.G., and S.C. performed the experiments; C.G., Z.C., D.J., X.Z., W.L., L.L., Y.W., B.-L.S., and D.W. designed the research; C.G., Z.C., D.J., and D.W. wrote the manuscript; and D.W. supervised the project.

DECLARATION OF INTERESTS

The authors declare no competing interests.

Received: February 12, 2018
Revised: July 25, 2018
Accepted: August 27, 2018
Published: October 23, 2018

REFERENCES

Bronner, D.N., Abuaita, B.H., Chen, X., Fitzgerald, K.A., Nuñez, G., He, Y., Yin, X.M., and O'Riordan, M.X. (2015). Endoplasmic reticulum stress activates the inflammasome via NLRP3- and caspase-2-driven mitochondrial damage. Immunity *43*, 451–462.

Brydges, S.D., Mueller, J.L., McGeough, M.D., Pena, C.A., Misaghi, A., Gandhi, C., Putnam, C.D., Boyle, D.L., Firestein, G.S., Horner, A.A., et al. (2009). Inflammasome-mediated disease animal models reveal roles for innate but not adaptive immunity. Immunity *30*, 875–887.

Cyster, J.G., Dang, E.V., Reboldi, A., and Yi, T. (2014). 25-Hydroxycholesterols in innate and adaptive immunity. Nat. Rev. Immunol. *14*, 731–743.

Dang, E.V., McDonald, J.G., Russell, D.W., and Cyster, J.G. (2017). Oxysterol restraint of cholesterol synthesis prevents AIM2 inflammasome activation. Cell *171*, 1057–1071.

DeBose-Boyd, R.A., Brown, M.S., Li, W.P., Nohturfft, A., Goldstein, J.L., and Espenshade, P.J. (1999). Transport-dependent proteolysis of SREBP: relocation of site-1 protease from Golgi to ER obviates the need for SREBP transport to Golgi. Cell *99*, 703–712.

Duewell, P., Kono, H., Rayner, K.J., Sirois, C.M., Vladimer, G., Bauernfeind, F.G., Abela, G.S., Franchi, L., Nuñez, G., Schnurr, M., et al. (2010). NLRP3 inflammasomes are required for atherogenesis and activated by cholesterol crystals. Nature *464*, 1357–1361.

Evavold, C.L., Ruan, J., Tan, Y., Xia, S., Wu, H., and Kagan, J.C. (2018). The Pore-forming protein gasdermin D regulates interleukin-1 secretion from living macrophages. Immunity *48*, 35–44.

Feng, L., Yan, H., Wu, Z., Yan, N., Wang, Z., Jeffrey, P.D., and Shi, Y. (2007). Structure of a site-2 protease family intramembrane metalloprotease. Science *318*, 1608–1612.

Gaidt, M.M., Ebert, T.S., Chauhan, D., Schmidt, T., Schmid-Burgk, J.L., Rapino, F., Robertson, A.A., Cooper, M.A., Graf, T., and Hornung, V. (2016). Human monocytes engage an alternative inflammasome pathway. Immunity *44*, 833–846.

Goldstein, J.L., DeBose-Boyd, R.A., and Brown, M.S. (2006). Protein sensors for membrane sterols. Cell *124*, 35–46.

Guarda, G., Braun, M., Staehli, F., Tardivel, A., Mattmann, C., Förster, I., Farlik, M., Decker, T., Du Pasquier, R.A., Romero, P., and Tschopp, J. (2011). Type I interferon inhibits interleukin-1 production and inflammasome activation. Immunity *34*, 213–223.

Guo, C., Xie, S., Chi, Z., Zhang, J., Liu, Y., Zhang, L., Zheng, M., Zhang, X., Xia, D., Ke, Y., et al. (2016). Bile acids control inflammation and metabolic disorder through inhibition of NLRP3 inflammasome. Immunity *45*, 944.

Gurcel, L., Abrami, L., Girardin, S., Tschopp, J., and van der Goot, F.G. (2006). Caspase-1 activation of lipid metabolic pathways in response to bacterial pore-forming toxins promotes cell survival. Cell *126*, 1135–1145.

Ichinohe, T., Pang, I.K., and Iwasaki, A. (2010). Influenza virus activates inflammasomes via its intracellular M2 ion channel. Nat. Immunol. *11*, 404–410.

Ito, A., Hong, C., Oka, K., Salazar, J.V., Diehl, C., Witztum, J.L., Diaz, M., Castrillo, A., Bensinger, S.J., Chan, L., and Tontonoz, P. (2016). Cholesterol accumulation in CD11c^{+} immune cells is a causal and targetable factor in autoimmune disease. Immunity *45*, 1311–1326.

Jang, J., Park, S., Jin Hur, H., Cho, H.J., Hwang, I., Pyo Kang, Y., Im, I., Lee, H., Lee, E., Yang, W., et al. (2016). 25-hydroxycholesterol contributes to cerebral inflammation of X-linked adrenoleukodystrophy through activation of the NLRP3 inflammasome. Nat. Commun. *7*, 13129.

Kamisuki, S., Mao, Q., Abu-Elheiga, L., Gu, Z., Kugimiya, A., Kwon, Y., Shinohara, T., Kawazoe, Y., Sato, S., Asakura, K., et al. (2009). A small molecule that blocks fat synthesis by inhibiting the activation of SREBP. Chem. Biol. *16*, 882–892.

Lordén, G., Sanjuán-García, I., de Pablo, N., Meana, C., Alvarez-Miguel, I., Pérez-García, M.T., Pelegrín, P., Balsinde, J., and Balboa, M.A. (2017). Lipin-2 regulates NLRP3 inflammasome by affecting P2X7 receptor activation. J. Exp. Med. *214*, 511–528.

Masters, S.L., Simon, A., Aksentijevich, I., and Kastner, D.L. (2009). Horror autoinflammaticus: the molecular pathophysiology of autoinflammatory disease (*). Annu. Rev. Immunol. *27*, 621–668.

Matsuda, M., Korn, B.S., Hammer, R.E., Moon, Y.A., Komuro, R., Horton, J.D., Goldstein, J.L., Brown, M.S., and Shimomura, I. (2001). SREBP cleavage-activating protein (SCAP) is required for increased lipid synthesis in liver induced by cholesterol deprivation and insulin elevation. Genes Dev. *15*, 1206–1216.

Menu, P., Mayor, A., Zhou, R., Tardivel, A., Ichijo, H., Mori, K., and Tschopp, J. (2012). ER stress activates the NLRP3 inflammasome via an UPR-independent pathway. Cell Death Dis. *3*, e261.

O'Neill, L.A., Kishton, R.J., and Rathmell, J. (2016). A guide to immunometabolism for immunologists. Nat. Rev. Immunol. *16*, 553–565.

Okada, T., Haze, K., Nadanaka, S., Yoshida, H., Seidah, N.G., Hirano, Y., Sato, R., Negishi, M., and Mori, K. (2003). A serine protease inhibitor prevents endoplasmic reticulum stress-induced cleavage but not transport of the membrane-bound transcription factor ATF6. J. Biol. Chem. *278*, 31024–31032.

Pearce, E.L., and Pearce, E.J. (2013). Metabolic pathways in immune cell activation and quiescence. Immunity *38*, 633–643.

Prinz, W.A. (2007). Non-vesicular sterol transport in cells. Prog. Lipid Res. *46*, 297–314.

Próchnicki, T., and Latz, E. (2017). Inflammasomes on the crossroads of innate immune recognition and metabolic control. Cell Metab. *26*, 71–93.

Radhakrishnan, A., Goldstein, J.L., McDonald, J.G., and Brown, M.S. (2008). Switch-like control of SREBP-2 transport triggered by small changes in ER cholesterol: a delicate balance. Cell Metab. *8*, 512–521.

Rathinam, V.A., and Fitzgerald, K.A. (2016). Inflammasome complexes: emerging mechanisms and effector functions. Cell *165*, 792–800.

Reboldi, A., Dang, E.V., McDonald, J.G., Liang, G., Russell, D.W., and Cyster, J.G. (2014). Inflammation. 25-Hydroxycholesterol suppresses interleukin-1-driven inflammation downstream of type I interferon. Science *345*, 679–684.

Sakai, J., Nohturfft, A., Goldstein, J.L., and Brown, M.S. (1998). Cleavage of sterol regulatory element-binding proteins (SREBPs) at site-1 requires interaction with SREBP cleavage-activating protein. Evidence from in vivo competition studies. J. Biol. Chem. *273*, 5785–5793.

Sato, R., Inoue, J., Kawabe, Y., Kodama, T., Takano, T., and Maeda, M. (1996). Sterol-dependent transcriptional regulation of sterol regulatory element-binding protein-2. J. Biol. Chem. *271*, 26461–26464.

Sattar, N., Preiss, D., Murray, H.M., Welsh, P., Buckley, B.M., de Craen, A.J., Seshasai, S.R., McMurray, J.J., Freeman, D.J., Jukema, J.W., et al. (2010). Statins and risk of incident diabetes: a collaborative meta-analysis of randomised statin trials. Lancet *375*, 735–742.

Shao, W., and Espenshade, P.J. (2014). Sterol regulatory element-binding protein (SREBP) cleavage regulates Golgi-to-endoplasmic reticulum recycling of SREBP cleavage-activating protein (SCAP). J. Biol. Chem. *289*, 7547–7557.

Sheedy, F.J., Grebe, A., Rayner, K.J., Kalantari, P., Ramkhelawon, B., Carpenter, S.B., Becker, C.E., Ediriweera, H.N., Mullick, A.E., Golenbock, D.T., et al. (2013). CD36 coordinates NLRP3 inflammasome activation by facilitating intracellular nucleation of soluble ligands into particulate ligands in sterile inflammation. Nat. Immunol. *14*, 812–820.

Spann, N.J., and Glass, C.K. (2013). Sterols and oxysterols in immune cell function. Nat. Immunol. *14*, 893–900.

Subramanian, N., Natarajan, K., Clatworthy, M.R., Wang, Z., and Germain, R.N. (2013). The adaptor MAVS promotes NLRP3 mitochondrial localization and inflammasome activation. Cell *153*, 348–361.

Tall, A.R., and Yvan-Charvet, L. (2015). Cholesterol, inflammation and innate immunity. Nat. Rev. Immunol. *15*, 104–116.

Tang, J.J., Li, J.G., Qi, W., Qiu, W.W., Li, P.S., Li, B.L., and Song, B.L. (2011). Inhibition of SREBP by a small molecule, betulin, improves hyperlipidemia and insulin resistance and reduces atherosclerotic plaques. Cell Metab. *13*, 44–56.

Triantafilou, K., Kar, S., van Kuppeveld, F.J., and Triantafilou, M. (2013). Rhinovirus-induced calcium flux triggers NLRP3 and NLRC5 activation in bronchial cells. Am. J. Respir. Cell Mol. Biol. *49*, 923–934.

Westerterp, M., Gautier, E.L., Ganda, A., Molusky, M.M., Wang, W., Fotakis, P., Wang, N., Randolph, G.J., D'Agati, V.D., Yvan-Charvet, L., et al. (2017). Cholesterol accumulation in dendritic cells links the inflammasome to acquired immunity. Cell Met. *25*, 1294–1304.

Yan, Y., Jiang, W., Spinetti, T., Tardivel, A., Castillo, R., Bourquin, C., Guarda, G., Tian, Z., Tschopp, J., and Zhou, R. (2013). Omega-3 fatty acids prevent inflammation and metabolic disorder through inhibition of NLRP3 inflammasome activation. Immunity *38*, 1154–1163.

York, A.G., Williams, K.J., Argus, J.P., Zhou, Q.D., Brar, G., Vergnes, L., Gray, E.E., Zhen, A., Wu, N.C., Yamada, D.H., et al. (2015). Limiting cholesterol biosynthetic flux spontaneously engages type I IFN signaling. Cell *163*, 1716–1729.

Youm, Y.H., Kanneganti, T.D., Vandanmagsar, B., Zhu, X., Ravussin, A., Adijiang, A., Owen, J.S., Thomas, M.J., Francis, J., Parks, J.S., and Dixit, V.D. (2012). The Nlrp3 inflammasome promotes age-related thymic demise and immunosenescence. Cell Rep. *1*, 56–68.

Zanoni, I., Tan, Y., Di Gioia, M., Broggi, A., Ruan, J., Shi, J., Donado, C.A., Shao, F., Wu, H., Springstead, J.R., and Kagan, J.C. (2016). An endogenous caspase-11 ligand elicits interleukin-1 release from living dendritic cells. Science *352*, 1232–1236.

Zhang, Z., Meszaros, G., He, W.T., Xu, Y., de Fatima Magliarelli, H., Mailly, L., Mihlan, M., Liu, Y., Puig Gámez, M., Goginashvili, A., et al. (2017). Protein kinase D at the Golgi controls NLRP3 inflammasome activation. J. Exp. Med. *214*, 2671–2693.

Zhou, R., Yazdi, A.S., Menu, P., and Tschopp, J. (2011). A role for mitochondria in NLRP3 inflammasome activation. Nature *469*, 221–225.

STAR★METHODS

KEY RESOURCES TABLE

REAGENT or RESOURCE	SOURCE	IDENTIFIER
Antibodies		
IL-1β	Cell Signaling	Cat# 12242; RRID: AB_2715503
IL-1β	R&D Systems	Cat# AF-401-NA; RRID: AB_416684
Caspase-1	Adipogen	Cat# AG-20B-0044 and AG-20B-0042; RRID: AB_2490253 and 2490248
NLRP3	Adipogen	Cat# AG-20B-0014; RRID: AB_2490202
ASC	Adipogen	Cat# AG-25B-0006; RRID: AB_2490440
SCAP	Santa Cruz	Cat# sc-9675; RRID: AB_656053
SREBP2	Abcam	Cat# ab30682; RRID: AB_779079
SREBP2	Santa Cruz	Cat# sc-13552 and sc-8151; RRID: AB_2194250 and 2194252
S1P	Abcam	Cat# ab140592
S2P	Abcam	Cat# ab140594
Flag	HuaAn biotechnology	Cat# 0912-1
V5	HuaAn biotechnology	Cat# M1008-2
Myc	HuaAn biotechnology	Cat# EM31105
HA	HuaAn biotechnology	Cat# 0906-1
β-actin	HuaAn biotechnology	Cat# M1210-2
Anti-Calreticulin	Abcam	Cat# ab92516; RRID: AB_10562796
Anti-Giantin	BioLegend	Cat# PRB-114C; RRID: AB_291560
SEC23A	NOVUS	Cat# NBP2-34842
GM130	Proteintech	Cat# 11308-1-AP; RRID: AB_2115327
β-tubulin	HuaAn biotechnology	em0103
VDAC1	Bioworld	BS6760
Ly6G	ebioscience	11-9668-80; RRID: AB_2572531
CD11b	ebioscience	E07073-1635
Bacterial and Virus Strains		
Salmonella	Prof. Yongqun Zhu	N/A
Biological Samples		
Healthy adult peripheral blood	Volunteers from Zhejiang University	N/A
Chemicals, Peptides, and Recombinant Proteins		
ATP	Sigma	A7699
LPS	Sigma	L2630
PMA	Sigma	P8139
25-HC	Sigma	H1015
Cholesterol	Sigma	C4951
Desmosterol	Sigma	D6513
Methyl-β-cyclodextrin	Sigma	C4555
Nigericin	Invivogen	tlrl-nig
MSU	Invivogen	tlrl-msu
poly-(dA:dT)	Invivogen	tlrl-patn

(*Continued on next page*)

Continued

REAGENT or RESOURCE	SOURCE	IDENTIFIER
Betulin	TargetMol	T3121
Fatostatin	TargetMol	T6832
Lovastatin	Selleck chemicals	S2061
z-VAD-FMK	Selleck chemicals	S7023
VX-765	Selleck chemicals	S2228
Nelfinavir Mesylate	Selleck chemicals	S4282
AEBSF	Selleck chemicals	S7378
Xanthohumol	Selleck chemicals	S7889
BFA	Biolegend	420601
PF429242	MedChem Express	HY-13447A
Alum	Thermo Fisher Scientific	77161
Mitotracker Deep Red	Invitrogen	1618702
1,10-Phenanthroline	Sigma	131377
Lipoprotein Deficient Serum from fetal calf	Sigma	S5394
(RS)-Mevalonic acid lithium salt $\geq$ 96.0% (GC)	Sigma	90469
Critical Commercial Assays		
IL-1β ELISA Kit	eBioscience	88-7013-77
IL-18 ELISA Kit	eBioscience	BMS618/3
TNFα ELISA Kit	eBioscience	88-7324-22
Duolink *In Situ* Red Starter Kit Goat/Rabbit 1kit	Sigma	DUO92105
Golgi Isolation Kit	Sigma	GL0010
Mitochondria/Cytosol Fractionation Kit	Biovision	K256-25
Amplex™ Red Cholesterol Assay Kit	Invitrogen	A12216
Experimental Models: Cell Lines		
HEK293T cells	ATCC	CRL-11268
THP1 cells	ATCC	TIB-202
J774A.1 cells	ATCC	TIB-67
iBMDM cells	Prof. Feng Shao	N/A
J774.1-shSCAP cells	This paper	N/A
THP-1-shSREBP2 cells	This paper	N/A
THP1-Flag-SREBP2 cells	This paper	N/A
THP1-V5-SCAP cells	This paper	N/A
Experimental Models: Organisms/Strains		
Mouse: C57BL/6	the Model Animal Research Center of Nanjing University	N000013
Mouse: *Scap*$^{f/f}$	Prof. Bao-Liang Song of Wuhan University.	N/A
Mouse: *Nlrp3*$^{-/-}$	Jackson Laboratory	JAX:021302
Mouse: *Mbtps1*$^{f/f}$	Jackson Laboratory	JAX:005994
Mouse: *Nlrp3*$^{A350V/neoR}$	Jackson Laboratory	JAX:017969
Mouse: *Lyz2-cre*	Jackson Laboratory	JAX:004781
Mouse: *Pycard*$^{-/-}$	Beijing Viewsolid Biotech	N/A
Mouse: *Casp1*$^{-/-}$	Beijing Viewsolid Biotech	N/A

(*Continued on next page*)

Continued

REAGENT or RESOURCE	SOURCE	IDENTIFIER
Oligonucleotides		
Mouse *Scap*-siRNA-1 (Sequence: 5′-CCAUGGCGACAUUACCUUGUA-3′)	This paper	N/A
Mouse *Scap*-siRNA-2 (Sequence: 5′-GCGUACAUCCAACAGAUAUUU-3′)	This paper	N/A
Mouse *Srebf2*-siRNA-1 (Sequence: 5′-GCGGACAACACACAAUAUCAU-3′)	This paper	N/A
Mouse *Srebf2*-siRNA-2 (Sequence: 5′-GAUGCUACAGUUUGUCAGCAA-3′)	This paper	N/A
Mouse *Mbtps1*-siRNA-1 (Sequence: 5′-CGGUACUCCAAAGUUCUUGAA-3′)	This paper	N/A
Mouse *Mbtps1*-siRNA-2 (Sequence: 5′-GCCUAUCUACUAUGGAGGAAU-3′)	This paper	N/A
Mouse *Mbtps2*-siRNA-1 (Sequence: 5′-GCAGCUAUUAGGGAACAAGUU-3′)	This paper	N/A
Mouse *Mbtps2*-siRNA-2 (Sequence: 5′-CCAGUGAUUGUGGAGACAUUU-3′)	This paper	N/A
Mouse *Mbtps2*-siRNA-3 (Sequence: 5′-GCGGAAAGCAAGGAUGCUU-3′)	This paper	N/A
Mouse *Mbtps2*-siRNA-4 (Sequence: 5′-GGAUUGUCCCGUUACUAAT-3′)	This paper	N/A
Mouse *Gapdh* primer forward: 5′-TGTGTCCGTCGTGGATCTGA-3′	This paper	N/A
Mouse *Gapdh* primer reverse: 5′-GCTTCACCACCTTCTTGAT-3′	This paper	N/A
Mouse *Srebf2* forward: 5′-GCGTTCTGGAGACCATGGA-3′	This paper	N/A
Mouse *Srebf2* reverse: 5′-ACAAAGTTGCTCTGAAAACAAATCA-3′	This paper	N/A
Mouse *Hmgcr* forward: 5′-CTTGTGGAATGCCTTGTGATTG-3′	This paper	N/A
Mouse *Hmgcr* reverse: 5′-AGCCGAAGCAGCACATGAT-3′	This paper	N/A
Mouse *Ldlr* forward: 5′-AGGCTGTGGGCTCCATAGG-3′	This paper	N/A
Mouse *Ldlr* reverse: 5′-TGCGGTCCAGGGTCATCT-3′	This paper	N/A
Mouse *Hmgcs1* forward: 5′-GCCGTGAACTGGGTCGAA-3′	This paper	N/A
Mouse *Hmgcs1* reverse: 5′-GCATATATAGCAATGTCTCCTGCAA-3′	This paper	N/A
Mouse *Insig1* forward: 5′-TCACAGTGACTGAGCTTCAGCA-3′	This paper	N/A
Mouse *Insig1* reverse: 5′-TCATCTTCATCACACCCAGGAC-3′	This paper	N/A
Mouse *Srebf1* forward: 5′-GGCCGAGATGTGCGAACT-3′	This paper	N/A
Mouse *Srebf1* reverse: 5′-TTGTTGATGAGCTGGAGCATGT-3′	This paper	N/A
Mouse *Acly* forward: 5′-GCCAGCGGGAGCACATC-3′	This paper	N/A
Mouse *Acly* reverse: 5′-CTTTGCAGGTGCCACTTCATC-3′	This paper	N/A
Mouse *Acaca* forward: 5′-TGACAGACTGATCGCAGAGAAAG-3′	This paper	N/A
Mouse *Acaca* reverse: 5′-TGGAGAGCCCCACACACA-3′	This paper	N/A
Mouse *Fasn* forward: 5′-GCTGCGGAAACTTCAGGAAAT-3′	This paper	N/A
Mouse *Fasn* reverse: 5′-AGAGACGTGTCACTCCTGGACTT-3′	This paper	N/A
Mouse *Acss2* forward: 5′-GCTGCCGACGGGATCAG-3′	This paper	N/A
Mouse *Acss2* reverse: 5′-TCCAGACACATTGAGCATGTCAT-3′	This paper	N/A
Mouse *Gpam* forward: 5′-CAACACCATCCCCGACATC-3′	This paper	N/A
Mouse *Gpam* reverse: 5′-GTGACCTTCGATTATGCGATCA-3′	This paper	N/A
Mouse *Scap* forward: 5′-ATTTGCTCACCGTGGAGATGTT-3′	This paper	N/A
Mouse *Scap* reverse: 5′-GAAGTCATCCAGGCCACTACTAATG-3′	This paper	N/A
Mouse *Abcg5* forward: 5′-TGGATCCAACACCTCTATGCTAAA-3′	This paper	N/A
Mouse *Abcg5* reverse: 5′-GGCAGGTTTTCTCGATGAACTG-3′	This paper	N/A
Mouse *Abca1* forward: 5′-CGTTTCCGGGAAGTGTCCTA-3′	This paper	N/A
Mouse *Abca1* reverse: 5′-GCTAGAGATGACAAGGAGGATGGA-3′	This paper	N/A
Recombinant DNA		
pcDNA3.1(-)-HA-ASC	This paper	N/A
pcDNA3.1(-)-myc-procaspase1	This paper	N/A
pcDNA3.1(-)-Flag-NEK7	This paper	N/A
pMX-S1P-KDEL	This paper	N/A
pMX-S1P-KDEL-S414A	This paper	N/A
GST-NLRP3-ΔPYD	Prof. Tao Li	N/A
NLRP3 R258W	This paper	N/A

(*Continued on next page*)

Continued

REAGENT or RESOURCE	SOURCE	IDENTIFIER
Software and Algorithms		
GraphPad Prism 6	GraphPad Software	N/A
Imaris 8.4	Core Facilities Zhejiang University School of Medicine	N/A
Flowjo	Core Facilities Zhejiang University School of Medicine	N/A

CONTACT REAGENTS AND RESOURCE SHARING

Further information and requests for resources and reagents should be directed to and will be fulfilled by the Lead Contact, Di Wang (diwang@zju.edu.cn).

EXPERIMENTAL MODEL AND SUBJECT DETAILS

Mice

C57BL/6 mice were purchased from the Model Animal Research Center of Nanjing University. *Scap*$^{f/f}$ mice were kindly provided by Prof. Bao-Liang Song of Wuhan University. *Nlrp3*$^{-/-}$, *Mbtps1*$^{f/f}$, *Nlrp3*^{A350VneoR}, and *Lyz2-cre* mice were purchased from the Jackson Laboratory. *Asc*$^{-/-}$ and *Casp1*$^{-/-}$ mice were purchased from Beijing Viewsolid Biotech. All mice were on the C57BL/6 background. *Scap*$^{f/f}$ and *Mbtps1*$^{f/f}$ mice were crossed with *Lyz2-cre* mice to obtain *Lyz2-cre-Scap*$^{f/f}$ and *Lyz2-cre-Mbtps1*$^{f/f}$ mice. All mice were housed in a specific pathogen-free facility in the University Laboratory Animal Center. Animal experimental protocols were approved by the Review Committee of Zhejiang University School of Medicine and were in compliance with institutional guidelines.

Cells

Mouse BMDMs were generated as previously described (Guo et al., 2016). Mouse peritoneal macrophages were collected 4 days after thioglycollate (Millipore) injection. iBMDMs, immortalized mouse macrophages (kindly provided by Prof. Feng Shao of National Institute of Biological Sciences, Beijing), and J774.1 cells were cultured in Dulbecco's modified Eagle's medium (DMEM) supplemented with 10% fetal bovine serum and 1% penicillin and streptomycin. THP-1 cells were cultured in RPMI 1640 containing the same supplements. THP-1 cells were differentiated for 3 hr with 100 nM phorbol myristate (PMA) and re-plated. PBMCs were isolated from peripheral blood from healthy volunteers who had given informed consent. Human monocyte-derived macrophages were generated from PBMCs purified from blood using Ficoll and cultured in RPMI-1640 medium containing 10% FBS and 1% penicillin-streptomycin and human GM-CSF (20 ng/mL, Peprotech) for 7 days.

For stimulation, 7×10^5 cells were plated in 12-well plates overnight, the medium was changed to opti-MEM the following morning, and then the cells were primed with LPS (500 ng/mL) for 4 hr. After that, the cells were stimulated with various NLRP3 activators [2 mM ATP (30 min); 10 μM nigericin (30 min); 200 μg/mL MSU (5 hr); 300 μg/mL alum (5 hr)]. For AIM2 inflammasome activation, poly(dA:dT) (1 μg/mL) was transfected using Lipofectamine 2000 (3 μl/μg DNA) following the manufacturer's protocol (Invitrogen). For NLRC4 inflammasome activation, *S. typhimurium* was grown overnight in Luria-Bertani broth, and BMDMs were infected for 1 hr with the *salmonella* culture (1:100) and then incubated for another 1 hr in the presence of gentamycin. Inhibitors were added 30 min or 1 hr before the inflammasome activators unless otherwise noted. Cell lysates and precipitated supernatants were analyzed by western blotting.

Reagents

ATP, LPS from *Escherichia coli* 0111:B4, PMA, 25-HC, cholesterol, desmosterol, and methyl-β-cyclodextrin were from Sigma; nigericin, MSU, and poly-(dA:dT) were from Invivogen; betulin and fatostatin were from TargetMol; lovastatin, z-VAD-FMK, VX-765, nelfinavir mesylate, AEBSF, and xanthohumol were from Selleck chemicals; BFA was from Biolegend; PF429242 was from MedChem Express; alum was from Thermo Fisher Scientific; and *Salmonella* was a kind gift from Prof. Yongqun Zhu of Zhejiang University.

The antibody against human IL-1β (12242) was from Cell Signaling; anti-IL-1β was from R&D Systems; anti-mouse caspase-1 (AG-20B-0044 and AG-20B-0042), anti-NLRP3 (AG-20B-0014), and anti-ASC (AG-25B-0006) were from Adipogen; anti-SCAP (sc-9675) was from Santa Cruz; anti-SREBP2 (ab30682), anti-S1P (ab140592), and anti-S2P (ab140594) were from Abcam; and anti-Flag (0912-1), anti-V5 (M1008-2), anti-Myc (EM31105), anti-HA (0906-1), and anti-β-actin (M1210-2) were from HuaAn biotechnology, Hangzhou, China.

METHOD DETAILS

Reconstitution of NLRP3 Inflammasome in HEK293T cells

HEK293T cells were seeded into 6-well plates at 5 × 10^5 per well in complete cell culture medium. After 24 hr, the cells were transfected with plasmids expressing Myc-pro-caspase-1 (500 ng), HA-ASC (150 ng), HA-NLRP3 (200 ng) and V5-SCAP (200 ng), using polyethylenimine. Forty-eight hours later, the cells were stimulated with nigericin for 30 min, and lysates were analyzed for the cleavage of pro-caspase-1 by western blotting.

Transfection and Co-Immunoprecipitation

Briefly, constructs were transfected into HEK293T cells using Polyethylenimine. After 24 hr, the cells were collected and resuspended in lysis buffer (50 mM Tris-Cl, 5 mM EDTA pH 7.4, 150 mM NaCl, 0.5% (vol/vol) Nonidet-P40, and 10% (vol/vol) glycerol) supplemented with 1 mM PMSF, 1 mM dithiothreitol (DTT), and complete protease inhibitor cocktail. Cell lysates were immunoprecipitated with the indicated antibody (after addition of protein A/G beads) overnight at 4°C and then immunocomplexes were washed three times in lysis buffer, resolved by SDS-PAGE, and analyzed by western blotting.

For two-step co-immunoprecipitation, HEK293T cells were transfected with V5–SCAP, Flag-SREBP2, and HA-NLRP3. After 24 hr, the cells were lysed with lysis buffer, and the lysates were incubated with anti-Flag M2 beads (Sigma) for 4 hr at 4°C. The beads were washed three times with elution buffer (50 mM Tris-Cl pH 7.5, 200 mM NaCl, 0.02% (vol/vol) Nonidet-P40, and 10% (vol/vol) glycerol) supplemented with 1 mM PMSF and 1 mM DTT, and the Flag-SREBP2 protein complex was eluted with 60 μL elution buffer containing 200 μg/mL 3 × Flag peptide (Sigma) for 1.5 hr at 4°C. Ten-microliter eluents were mixed with 2 × SDS loading as the first immunoprecipitation elution for western blotting. For the second immunoprecipitation, 450 μL lysis buffer containing anti-V5 antibody with protein A/G beads was mixed with the remaining 50 μL eluent from the first immunoprecipitation, incubated with rotation overnight at 4°C, and then the immunocomplexes were washed three times in lysis buffer, resolved by SDS-PAGE, and analyzed by western blotting.

ASC Oligomerization and ASC Speck Formation

BMDMs were plated in six-well plates (2 × 10^6 cells per well) and then stimulated with 500 ng/mL LPS for 4 hr the following day. Cells were treated with 10 μM nigericin for 45 min in the presence of the indicated inhibitors. The supernatants were removed, the cells were rinsed in ice-cold phosphate-buffered saline (PBS), and 500 μL ice-cold buffer (50 mM Tris-HCl pH 7.6, 0.5% Triton X-100, 0.1 mM PMSF, and a protease inhibitor cocktail) was added. Cells were scraped and lysed by shearing 10 times through a 21-gauge needle, then 50 μL of lysate was removed for western blot analysis. Lysates were centrifuged at 330 × g for 10 min at 4°C and pellets were washed twice in ice-cold PBS and re-suspended in 500 μL PBS. Disuccinimidyl suberate (2mM) was added to the re-suspended pellets, which were incubated at room temperature for 30 min with rotation. Samples were then centrifuged and the cross-linked pellets were re-suspended in 60 μL SDS sample buffer. Samples were boiled for 5 min at 99°C and analyzed by western blotting.

For ASC speck formation, BMDMs were seeded at 5 × 10^5/mL on chamber slides and allowed to attach overnight. The following day, the cells were primed with LPS and treated with nigericin in the presence or absence of the indicated inhibitors. The cells were fixed in 4% paraformaldehyde followed by ASC and DAPI staining.

Small-interfering RNA Transfection

Peritoneal macrophages were plated in 12-well plates (3 × 10^5 cells per well) and then transfected with 100 nM siRNA using Lipofectamine RNAiMAX (Thermo Fisher Scientific) according to the manufacturer's instructions. The siRNA sequences for mouse SCAP (#1: 5′-CCAUGGCGACAUUACCUUGUA-3′; #2: 5′-GCGUACAUCCAACAGAUAUUU-3′), SREBP2 (#1:5′-GCGGACAACACACAAUAUCAU-3′; #2: 5′-GAUGCUACAGUUUGUCAGCAA-3′), S1P (#1: 5′-CGGUACUCCAAAGUUCUUGAA-3′; #2: 5′-GCCUAUCUACUAUGGAGGAAU-3′), S2P (#1: 5′-GCAGCUAUUAGGGAACAAGUU-3′; #2: 5′-CCAGUGAUUGUGGAGACAUUU-3′; #3: 5′-GCGGAAAGCAAGGAUGCUU-3′; #4: 5′-GGAUUGUCCCGUUACUAAT-3′) and the indicated scrambled siRNAs were chemically synthesized by Genepharma Co., Shanghai, China.

Cellular Fractionation

Cytosol and mitochondria were isolated from THP-1 cells stably overexpressing V5-SCAP using a Mitochondria and Cytosol fractionation Kit (K256; Biovision) according to the manufacturer's guidelines. Isolation of the Golgi apparatus was performed using a Golgi isolation kit (GL0010; Sigma- Aldrich) according to the manufacturer's protocol.

Quantitative PCR

RNA was extracted using RNAiso Plus reagent (Takara). Complementary DNA was synthesized with Oligo-dT primer using the SuperScript First-Strand cDNA Synthesis kit (Vazyme Biotech) according to the manufacturer's protocols. Quantitative PCR was performed using SYBR Green (Vazyme Biotech) on a LightCycler 480 (Roche Diagnostics). The samples were individually normalized to *GAPDH*. The following primers were used: *Gapdh* forward: 5′-TGTGTCCGTCGTGGATCTGA-3′, reverse: 5′-GCTTCACCACCTTCTTGAT-3′; *Srebf2* forward: 5′-GCGTTCTGGAGACCATGGA-3′, reverse: 5′-ACAAAGTTGCTCTGAAAACAAATCA-3′; *Hmgcr*

forward: 5′-CTTGTGGAATGCCTTGTGATTG-3′, reverse: 5′-AGCCGAAGCAGCACATGAT-3′; *Ldlr* forward: 5′-AGGCTGTGGGCTC CATAGG-3′, reverse: 5′-TGCGGTCCAGGGTCATCT-3′; *Hmgcs1* forward: 5′-GCCGTGAACTGGGTCGAA-3′, reverse: 5′-GCATAT ATAGCAATGTCTCCTGCAA-3′; *Insig1* forward: 5′-TCACAGTGACTGAGCTTCAGCA-3′, reverse: 5′-TCATCTTCATCACACCCAG GAC-3′; *Srebf1* forward: 5′-GGCCGAGATGTGCGAACT-3′, reverse: 5′-TTGTTGATGAGCTGGAGCATGT-3′; *Acly* forward: 5′-GCCA GCGGGAGCACATC-3′, reverse: 5′-CTTTGCAGGTGCCACTTCATC-3′; *Acaca* forward: 5′-TGACAGACTGATCGCAGAGAAAG-3′, reverse: 5′-TGGAGAGCCCCACACACA-3′; *Fasn* forward: 5′-GCTGCGGAAACTTCAGGAAAT-3′, reverse: 5′-AGAGACGTGTCACTC CTGGACTT-3′; *Acss2* forward: 5′-GCTGCCGACGGGATCAG-3′, reverse: 5′-TCCAGACACATTGAGCATGTCAT-3′; *Gpam* forward: 5′-CAACACCATCCCCGACATC-3′, reverse: 5′-GTGACCTTCGATTATGCGATCA-3′; *Scap* forward: 5′-ATTTGCTCACCGTGGAGA TGTT-3′, reverse: 5′-GAAGTCATCCAGGCCACTACTAATG-3′; *Abcg5* forward: 5′-TGGATCCAACACCTCTATGCTAAA-3′, reverse: 5′-GGCAGGTTTTCTCGATGAACTG-3′; *Abca1* forward: 5′-CGTTTCCGGGAAGTGTCCTA-3′, reverse: 5′-GCTAGAGATGACAAGG AGGATGGA-3′.

Total Cholesterol Assessment

Macrophages were lysed with RIPA buffer. Fifty microliters of lysate was transferred to a dark-walled, clear-bottom 384-well dish and then incubated with 50 μL cholesterol detecting reagent-Amplex Red (Invitrogen) for 30 min at 37°C. Fluorescence intensity was measured by a microplate reader.

Immunofluorescence Staining and Confocal Microscopy

Under transient low-expression conditions, HEK293T cells were transfected with 100 ng plasmid as indicated for 12 hr, and stimulated with 10 μM Nigericin for 30 min. BMDMs were stained for 30 min at 37°C with 400 nM Mitotracker Deep Red (Invitrogen). After washing twice with PBS, the cells were fixed in 4% paraformaldehyde in PBS for 20 min and then washed three times in PBS with Tween 20 (PBST). After permeabilization with Triton X-100 and blocking with 5% bovine serum albumin in PBS, the cells were incubated with primary antibodies overnight at 4°C. After washing with PBST, the cells were incubated with secondary antibodies (Sigma) in PBS for 30 min and rinsed in PBST. Analyses were carried out using a Nikon A1R confocal microscope.

Super-resolution Microscopy and Structured Illumination Microscopy

Sample preparation was as described above. For three-dimensional reconstruction, images of BMDMs were captured using Nikon-Structured Illumination Microscopy (N-SIM); the microscope was an ECLIPSE Ti and the objective lens was a CFI Apochromat TIRF 100XH. Images were recorded as vertical z stacks and processed using NIS analysis and Imaris 8.4 software to generate three-dimensional images and movies.

Proximity Ligation Assay

Proximity ligation assays were performed using Duolink reagents (Sigma) according to the manufacturer's instructions.

Virus Transduction of THP1 and J774.1 Macrophages

THP1 macrophages were spinfected with retrovirus encoding Flag-SREBP2 or lentivirus encoding V5-SCAP for 90 min at 2500 rpm and 32°C. Forty-eight hours after infection, the cells were selected by culture with 2 μg/mL puromycin (Sigma) or blasticidin (Invivogen). The shRNAs targeting *SCAP* and *SREBP2* were from Sigma. J774.1-shSCAP and THP-1-shSREBP2 cells were also generated by spinfection and selected with puromycin.

ELISA

Supernatants from cell cultures and sera were collected and the concentrations of IL-1β, IL-18, and TNFα (all from eBioscience) were determined according to the manufacturer's instructions.

Liposomal-Cholesterol Preparation

Briefly, 5.8 mg cholesterol and 8 mg PC were placed in chloroform, and a thin film were prepared; subsequently, it was placed in 1 mL RPMI-1640 medium and was sonicated at 4°C.

Sterol-Depletion Experiments

For *in vitro* experiments, BMDMs were cultured in DMEM supplemented with 10% lipoprotein-deficient serum (LPDS, Sigma), 10 μM lovastatin, and 50 μM mevalonate for 16 hr. Then the cells were primed with LPS and stimulated with nigericin. For *in vivo* experiment, C57BL/6 mice at 6 weeks of age were fed with a normal chow diet or a chow diet supplemented with 0.2% (wt/wt) lovastatin for 4 days. On day 5, the mice were challenged with LPS or alum.

In Vivo LPS Challenge

C57BL/B6 mice were injected intraperitoneally with LPS (20 mg/kg body weight) alone or LPS plus betulin (30 mg/kg), fatostatin (20 mg/kg), desmosterol (30 mg/kg), or 25-HC (50 mg/kg). After 4 hr the mice were killed, and the serum concentrations of IL-1β, IL-18, and TNFα were measured by ELISA.

Alum-Induced Peritonitis

To create peritonitis models, mice were injected intraperitoneally with 2 mg alum dissolved in 0.2 mL sterile PBS; 6 hr later, the mice were killed and the peritoneal cavity washed with cold PBS. The peritoneal lavage fluid was analyzed using FACS Calibur for the recruitment of polymorphonuclear neutrophils with the neutrophil markers Ly6G (RB6-8C5, ebioscience) and CD11b (M1/70, ebioscience), and IL-1β production was determined by ELISA.

QUANTIFICATION AND STATISTICAL ANALYSIS

The results are expressed as the mean ± SD. Statistical analysis was carried out using Student's t test for two groups or the Kaplan-Meier method for mouse survival as indicated using GraphPad Prism, unless otherwise noted. Differences were considered significant when $^{*}p \leq 0.05$, $^{**}p \leq 0.01$, $^{***}p \leq 0.001$.